https://doi.org/10.5194/wes-2024-12
Preprint. Discussion started: 13 February 2024

eawe european academy of wind energy
Open Access WIND ENERGY SCIENCE DISCUSSIONS

Data assimilation of realistic boundary-layer flows for wind-turbine applications - An LES study

Linus Wrba[1], Antonia Englberger[1], Andreas Dörnbrack[1], Gerard Kilroy[1], and Norman Wildmann[1]
[1]Deutsches Zentrum für Luft- und Raumfahrt, Institut für Physik der Atmosphäre, Oberpfaffenhofen, Germany
Correspondence: Linus Wrba (linus.wrba@dlr.de)

Abstract. Providing observed date- and site-specific turbulent inflow fields for Large-eddy simulations (LES) of the flow through wind turbines becomes more and more important for realistic estimates of power production. In this study, data assimilation techniques are used to adapt the atmospheric inflow field towards measurement data. A Newtonian relaxation technique and a vibration assimilation method are implemented in the geophysical flow solver EULAG. Their capability of adapting mean wind profiles towards field measurements while maintaining the atmospheric turbulence of an idealized LES is investigated. The sensitivity of the methods to grid refinement and to parameter changes is analysed. The performance of the vibration assimilation technique is better suited for fine grids (dx=dy=dz=5 m) because of smaller damping effects on the atmospheric turbulence. Furthermore, the vibration method is used to nudge the inflow field of an idealized atmospheric simulation towards velocity profiles measured at the wind-farm site WiValdi at Krummendeich. A near neutral stratification is chosen from the measurements to test the assimilation technique. With the vibration assimilation method it is possible to adapt the zonal and meridional velocity components of an atmospheric flow. The LESs applying data assimilation are compared with the measurements and independent mesoscale simulations. A good accordance is found for the mean inflow velocity profiles and the turbulence intensities. In a final step, the assimilated flow field is taken as inflow for a wind-turbine simulation. The wind-turbine simulation shows characteristic structures of a wake in the atmospheric boundary layer. This study demonstrates that an efficient computing of different and realistic inflow fields for wind-turbine simulations is possible applying the vibration assimilation method.

Keywords: LES, data assimilation, atmospheric boundary layer, wind-turbine wake

1 Introduction

The growing demand for wind energy is accompanied with a wide range of challenges as structural and technical characteristics of wind turbines are getting more and more sophisticated. Especially, the interaction of wind turbines wakes in wind farms and their response to the transient atmospheric flow field are grand challenges in wind energy research (cf. Veers et al. (2023)).

https://doi.org/10.5194/wes-2024-12
Preprint. Discussion started: 13 February 2024

eawe european academy of wind energy
Open Access WIND ENERGY SCIENCE DISCUSSIONS

General attention is laid on the performance and the loads on the blades which are mainly controlled by the turbulence in the atmosphere (cf. Hansen (2013), Wharton and Lundquist (2012)). The crucial question is, how much power can be harvested at a certain location with a specific configuration of wind turbines. The atmospheric situation during which wind turbines are operating has to be involved in such considerations because rotor diameters and hub heights are increasing and cover a wide depth of the atmospheric boundary layer (ABL). A better knowledge of the impact of different atmospheric characteristics like vertical gradient of the horizontal velocity and turbulence intensities on the wake behind a wind turbine is therefore essential.

Either field measurements or numerical simulations can provide the required information about the flow field surrounding a rotor. LES models have been proven a useful tool to compute turbulent flow fields. In contrast to simulations based on Reynolds averaged Navier-Stokes (RANS) equations, LESs are capable of resolving turbulence partially in the flow. In addition, LESs are computationally less expensive than direct numerical simulations (DNS) because the subgrid-scale (SGS) contribution to the turbulence is parameterized. LESs are widely used in literature in order to assess the impact of the atmospheric stratification on wind turbines and wind farms. The beginnings of LESs for the purpose of meteorological applications lay in the 1960s and 1970s (e.g. Lilly (1965) and Deardorff (1974)). With the increasing importance of wind power for the energy sector, wind turbines have been included frequently in LES (cf. Porté-Agel et al. (2020)). Troldborg et al. (2007) revealed that a higher atmospheric turbulence leads to a more rapid wake recovery. Further research considered the differences in the flow during the diurnal cycle. The behavior of the wake for a stable stratified nighttime boundary layer has been investigated numerically by e.g. Lu and Porté-Agel (2011), Bhaganagar and Debnath (2014, 2015) and Abkar and Porté-Agel (2015) as well as for the diurnal cycle (cf. Abkar et al. (2016) and Englberger and Dörnbrack (2018)). These studies show a less rapid wake recovery under stable conditions during night than under convective conditions during day.

There are different numerical approaches for the generation of turbulent inflow fields for wind-turbine simulations. One possibility are synthetic turbulence fields which were proposed by Mann (1994). With these stochastic models high computational costs can be avoided but they are not physical models in a sense that they satisfy the conservation laws (cf. Naughton et al. (2011)). Atmospheric inflow fields which are more close to reality are generated by LESs. Idealized atmospheric flow simulations which are computed without a wind turbine are often used to provide inflow fields for in wind-turbine simulations (cf. Bhaganagar and Debnath (2014), Abkar et al. (2016), Englberger and Dörnbrack (2017)). These atmospheric precursor simulations are computationally expensive because turbulence has to spin up in the regarded domain until the key flow parameters (vertical gradient of horizontal velocity, turbulence intensity) match anticipated characteristics in the ABL. Furthermore, most of these simulations are conducted for idealized flow conditions in the ABL and often deviate from actual atmospheric situations. This is a disadvantage for a reliable prediction of the energy gain at a certain location because the loads on the blades are very sensitive to mesoscale inflow conditions, for example orographically-induced deviations from these idealized inflow. Realistic site-specific three-dimensional simulations are necessary for the analysis of wind energy plants for varying ABL flow regimes. However, it is still challenging to simulate regional or local flow fields by LES.

One option for the generation of site-specific atmospheric inflow conditions is the coupling of mesoscale simulations (e.g. simulations of the weather research and forecasting model (WRF)) with the microscale simulation (LES). Recent experience

https://doi.org/10.5194/wes-2024-12
Preprint. Discussion started: 13 February 2024

eawe european academy of wind energy
Open Access WIND ENERGY SCIENCE DISCUSSIONS

on this research field has been made in the Mesoscale to Microscale Coupling (MMC) project sponsored by the U.S. Department of Energy (cf. Haupt et al. (2022)). The authors are emphasizing the complexity of modeling the energy transfer from the largest scales of the atmosphere to those scales inside the ABL where wind turbines extract energy. Simulations from the mesoscale down to the microscale (for example with WRF-LES) are very computational expensive.

The consideration of wind and temperature observations in LESs would be a logical way to introduce realistic data into high-resolution simulations of turbulent flow. However, it is quite challenging to run simulations accounting for all previously defined conditions (initial conditions, surface boundary conditions, large-scale forcing) to match the observed flow parameters (cf. Allaerts et al. (2023)). Detailed observational data from atmospheric situations is also spatially and temporally limited. Furthermore, site-specific measurements show in general similar flow characteristics for one stratification and a main wind direction and only small differences in the hub-height wind speed, the vertical gradient of the velocity and the atmospheric turbulence.

Data Assimilation is a possibility to keep simulated flow parameters like wind speed and potential temperature close to measurement data. In the WRF model (cf. Skamarock et al. (2019)) different four-dimensional data assimilation schemes developed by Stauffer and Seaman (1990) are implemented. Concerning microscale simulations, an advantage of this approach would be the combination of the resolved turbulence in the LES with real data observed at specific locations. However, there are some difficulties when data assimilation methods are used in high resolved simulations. The methods have usually damping effects on the atmospheric turbulence due to the averaged variables which are used for the assimilation and do not account for fluctuations. Neggers et al. (2012) and Maronga et al. (2015) noted that the use of the Newtonian relaxation method (often called nudging) implies a relaxation timescale to be large enough to allow turbulence development but also small enough for an adequate forcing. Allaerts et al. (2020) recently developed the profile-assimilation technique which consists of a proportional gain controller taking as input the time-height history of mean-flow quantities. Nakayama and Takemi (2020) developed an advanced assimilation technique based on the vibration equation for the velocity oscillating around a zero-wind basic state with a certain frequency. They pointed out the advantage of this method in terms of turbulence intensity handling.

With this study we want to make a step towards more realistic date- and site-specific inflow fields for wind-turbine LESs using data assimilation techniques. This will lead to a better knowledge of wakes behind wind turbines in less idealized and more realistic conditions and wind farm provider will be able to predict the energy gain and the loads at the rotor blades more precisely using the developed methods. The main objective of this study is the computational efficient generation of realistic atmospheric inflow fields with arbitrary velocity profiles based on observational data for wind turbines in LESs. Measurement data from the research wind farm site WiValdi (https://windenergy-researchfarm.com/) at Krummendeich in the North of Germany and averaged WRF profiles will be used for a comparative analysis. The following outstanding scientific questions will be considered:

1. Which of the considered assimilation method is able to preserve turbulence?
2. Can velocities taken from idealized atmospheric precursor simulations be assimilated towards arbitrary measured wind profiles?

https://doi.org/10.5194/wes-2024-12
Preprint. Discussion started: 13 February 2024

eawe european academy of wind energy
Open Access WIND ENERGY SCIENCE DISCUSSIONS

3 How does the wake behind a wind turbine change between idealized and more realistic inflow conditions?

The outline of this publication is as follows. The numerical model EULAG, the considered assimilation methods, the measurements and the setup for the precursor simulations are presented in Sect. 2. In Sect. 3 the Newtonian relaxation and the assimilation technique with the vibration equation are compared for the idealized example presented by Nakayama and Takemi (2020) with dx=dy=40 m and dy=10 m. Subsequently in Sect. 4, both assimilation methods are tested for a finer grid spacing (dx=dy=dz=5 m) and differences compared to the coarse case are examined. In Sect. 5 a site specific inflow field is computed for the wind farm site WiValdi by assimilation of an idealized precursor flow field. In Sect. 6 the assimilation of a precursor simulation is combined with the simulation of the wake behind a wind turbine. Conclusions are given in Sect. 7.

2 Methodology

2.1 The Numerical Model EULAG

The dry and incompressible atmospheric flow as well as the flow through a wind turbine are modelled with the geophysical flow solver EULAG. EULAG is an established computational model which is used for a wide range of physical scenarios (cf. Prusa et al. (2008)). It has been used for the simulation of urban flows (Smolarkiewicz et al. (2007)), gravity waves (Smolarkiewicz and Dörnbrack (2008)), turbulent atmospheric flows (Margolin et al. (1999)) and even solar convection (Elliott and Smolarkiewicz (2002)). The name EULAG refers to the two possible ways to solve the equations of motion either in **EU**lerian (flux form) (cf. Smolarkiewicz and Margolin (1993)) or in semi-**LAG**rangian (advective form) (cf. Smolarkiewicz and Pudykiewicz (1992)) mode. The advective terms in the fluid equations are approximated by the iterative finite-difference algorithm MPDATA (multidimensional positive definite advection transport algorithm) which is second-order accurate, positive definite, conservative, and computationally efficient (cf. Smolarkiewicz and Margolin (1998)). A detailed explanation of EULAG can be found in Smolarkiewicz and Margolin (1998) and Prusa et al. (2008).
For the simulations in this study, the following set of non-hydrostatic Boussinesq equations with constant density $\rho_0 = 1.1\ \mathrm{kg\ m^{-3}}$ are solved for the Cartesian velocity components $\boldsymbol{v} = (u, v, w)$ and for the potential temperature perturbation $\Theta' = \Theta - \Theta_e$ (cf. Smolarkiewicz et al. (2007) and Englberger and Dörnbrack (2018)):

$$\boldsymbol{\nabla} \cdot \boldsymbol{v} = 0 \quad , \tag{1}$$

$$\frac{d\boldsymbol{v}}{dt} = \underbrace{-\boldsymbol{\nabla}\left(\frac{p'}{\rho_0}\right)}_{\text{pressure gradient}} + \underbrace{\boldsymbol{g}\frac{\Theta'}{\Theta_0}}_{\text{buoyancy}} - \underbrace{2\Omega(\boldsymbol{v} - \boldsymbol{v}_e)}_{\text{Coriolis-Force } \mathbf{F}_{\text{cor}}} + \underbrace{\frac{\boldsymbol{F}}{\rho_0}}_{\boldsymbol{F}_{WT}} - \mathbf{f} + \mathbf{V} \quad , \tag{2}$$

$$\frac{d\Theta'}{dt} = -\boldsymbol{v}\boldsymbol{\nabla}\Theta_{\mathrm{e}} + \mathbf{H} \quad . \tag{3}$$

https://doi.org/10.5194/wes-2024-12
Preprint. Discussion started: 13 February 2024

eawe european academy of wind energy
Open Access WIND ENERGY SCIENCE DISCUSSIONS

In these equations Θ_0 denotes the constant reference value and Θ_e the balanced ambient environment state. $\frac{d}{dt}$, $\boldsymbol{\nabla}$ and $\boldsymbol{\nabla}\cdot$ represent the total derivative, the gradient and the divergence. p' symbolizes the pressure perturbations, $\boldsymbol{g} = (0, 0, -g)$ is the acceleration due to gravity and $\mathbf{F}_{cor}$ indicates the Coriolis force with the angular velocity vector of the earth's rotation Ω. $\mathbf{V}$ and $\mathbf{H}$ are subgrid-scale (SGS) terms and indicate turbulent dissipation of momentum and diffusion of heat. The simulations within this study are all conducted with a turbulence kinetic energy (TKE) closure (cf. Margolin et al. (1999)). $\mathbf{f}$ denotes the additional forcing due to data assimilation. In the simulations with wind turbines, $\mathbf{F}_{WT}$ corresponds to the forces generated by the rotor blades. The wind turbine is implemented with the blade-element momentum theory as a rotating actuator disc (cf. Mirocha et al. (2014); Englberger and Dörnbrack (2017)). Unfortunately, the blade data necessary for the calculation of the forces on the flow induced by the blades is at the moment not available for the Enercon E-115 EP3 ($h_{hub} = 92$ m, rotor diameter $D = 116$ m) which is built in Krummendeich. Therefore, the simulations are conducted with the 5 MW reference wind turbine defined by the National Renewable Energy Laboratory (NREL) (Jonkman et al. (2009)). This wind turbine has a similar hub height ($h_{hub} = 90$ m) and rotor diameter ($D = 126$ m).

2.2 Assimilation Methods

There are several factors limiting the accuracy and comparability of LESs with real case measurements and field observations. On the one hand, the truncation errors due to discretization which are necessary for the calculation of the solution are limiting the accuracy of the numerical model (cf. Arcucci et al. (2017); Neggers et al. (2012)). On the other hand, many meteorological effects on small scales occurring due to mesoscale phenomena, e.g. frontal passages, atmospheric waves and diurnal land–sea breezes, can't be represented correctly by LESs (cf. Allaerts et al. (2020)). As simulations with wind turbines are concerned, the grid spacing has to be small enough to account for forces generated at the blades. Considering a stable boundary layer (SBL), the turbulent scales within this atmospheric stratification are very small and can only be resolved with a fine grid spacing (dx=dy=dz=5 m). Therefore, the domain size is restricted to the order of kilometers and mesoscale phenomena can't be represented within these simulations, as their scales range from 10 km to more than 100 km (Haupt et al. (2022)).

Data assimilation techniques are widely used in many numerical models in order to improve simulation accuracy and for the assimilation of the flow field of the simulations towards observational data. For example, in WRF a grid-nudging method is implemented based on the four-dimensional data assimilation developed by Stauffer and Seaman (1990). This scheme relies on the definition of the Newtonian relaxation

$$\left.\frac{\delta \Phi}{\delta t}\right|_{NUD} = -\frac{\Phi - \Phi_{target}}{\tau} \quad . \tag{4}$$

In this equation Φ is a variable like velocity, temperature or concentration and Φ_{target} symbols its target value given through observational data. τ is the relaxation time scale which has to be chosen small enough to generate a considerable forcing towards the target data but not too small that small-scale atmospheric turbulence is suppressed (cf. Neggers et al. (2012); Maronga et al. (2015)). The severe drawback of this method is the damping of small-scale turbulent structures in the atmosphere which is mentioned by Neggers et al. (2012), Maronga et al. (2015), Heinze et al. (2017), Nakayama and Takemi (2020).

Nakayama and Takemi (2020) proposed a different way of assimilating velocities in LESs based on the vibration equation

https://doi.org/10.5194/wes-2024-12
Preprint. Discussion started: 13 February 2024

eawe european academy of wind energy
Open Access WIND ENERGY SCIENCE DISCUSSIONS

for the velocity oscillating around a zero-wind basic state with a certain frequency. They showed that their method preserves turbulent fluctuations well and can still approximate velocities to measured wind profiles. The following forcing term is derived from the vibration equation

$$\mathbf{f}(x,y,z,t) = damp(x)\rho_0\omega_0^2 \int_0^t (u(x,y,z,t') - U_{OBS}(z,t'))dt' \tag{5}$$

with

$$damp(x) = \sin^2\left[\frac{\pi}{2}\left(1 - \frac{x_{\text{nud}} - x}{x_l}\right)\right] \quad , \quad x_{\text{nud}} - \frac{x_l}{2} \leq \quad x \quad \leq x_{nud} + \frac{x_l}{2} \quad . \tag{6}$$

f symbolizes the forcing term additionally introduced in the equation for the conservation of momentum (Eq. 2). u and U_{OBS} correspond to the instantaneous wind velocity at a certain grid point and the averaged observational velocity at the related height, respectively. ρ is the density and ω_0 the frequency for the oscillating velocity in the vibration equation. $damp(x)$ is a Gaussian damping function in the streamwise direction to prevent numerical artefacts at the borders of the nudging area. x_{nud} is the center of nudging area in and x_l the length of the damping layer for the streamwise direction.

2.3 Measurement Data

Since November 2020, a long-range, scanning Doppler wind lidar (DWL) is installed at the WiValdi site to measure vertical profiles of wind speed and direction over the entire height of the ABL. The DWL is configured to measure in a velocity azimuth display (VAD) mode with a high angular resolution and a specific elevation angle to obtain accurate measurements of the mean wind vector profile as well as TKE and its dissipation rate (Wildmann et al. (2020)). A microwave radiometer is installed along-side to obtain temperature and humidity profiles as well. With this combination of instruments long-term statistics and typical characteristics of atmospheric conditions at the site can be determined (Wildmann et al. (2022)). For the comparison of the assimilated velocities in the idealized precursor simulation in Sect. 5, as situation was chosen the 19.11.2021 18 UTC to 19 UTC which features strong wind shear near to the ground and a larger wind veer in the boundary layer.

2.4 Precursor Simulations

The numerical simulations are separated into a precursor simulation and a simulation with data assimilation (+ wind turbine simulation). Table 1 gives an overview of all simulations which are conducted during this study. Figure 1 shows a schematic illustration of the simulation approach used in this study. In the first precursor simulation P1, a fully developed flow corresponding to a neutral boundary layer (NBL) with the zonal velocity profile $u = u_*(\frac{z}{z_0})^n$ (friction velocity $u_* = 0.45$ m s^{-1}, roughness length $z_0 = 0.1$ m and exponent $n = 0.14$) is achieved by the application of a constant pressure gradient in the horizontal direction. The pressure gradient is implemented as an additional forcing $-u_*^2/H$ in Eq. 2 with the friction velocity and the domain height $H = 1000$ m. For the surface friction the drag coefficient in the surface parametrization is set to 0.017. 150000 time steps with $\Delta t = 1$ s are calculated on 100 processors in 25 physical hours for this precursor simulation to develop

https://doi.org/10.5194/wes-2024-12
Preprint. Discussion started: 13 February 2024

eawe european academy of wind energy
Open Access WIND ENERGY SCIENCE DISCUSSIONS

an equilibrium. For the comparison to the investigation of Nakayama and Takemi (2020) the domain size was identically set to 6000 x 6000 x 1000 m^3 with a grid spacing of dx = dy = 40 m and dz = 10 m. The precursor simulation is performed with periodic boundary conditions in the horizontal directions and an open boundary condition at the top of the domain. The Coriolis-parameter is set to zero. For the following simulation with data assimilation 2D yz-slices are extracted at $x = 3000$ m at each time step after the simulation has reached a quasi-equilibrium state. 1050 2D slices from the three velocity components and the potential temperature perturbation were taken as input at the inlet of the nudging simulation. Here, the boundary conditions in the horizontal directions and at the top are open, the additional pressure gradient term is excluded and the accelerations due to earth rotation are turned on.

As wind-turbine simulations require a higher resolution we performed another precursor simulation P2 for the same NBL conditions like in P1. The grid spacing for this simulation is dx = dy = dz = 5 m. A smaller domain is chosen in order to reduce the calculation time and it is set to 3000 x 3000 x 1000 m^3. The boundary conditions in horizontal direction remain periodic and the drag coefficient is decreased to 0.01 to fit for the velocity profile prescribed by the power law in P1. At the top of the domain the boundary condition is open. 6000 2D yz-slices are extracted from this precursor simulation for the input of the nudging simulation. The presented precursor simulations are used for the assessment of the different assimilation methods which are explained in Sect. 2.2.

A third precursor simulation P3 is assessed in this study to test the assimilation technique. The atmospheric condition in this simulation corresponds to a stable stratification. This precursor simulation was developed by Englberger and Dörnbrack (2018) during their investigation of the impact of different stratifications on wind-turbine wakes. The domain size of this SBL is 5120 x 2560 x 320 m^3 with a grid spacing of dx = dy = dz = 5 m.

In this study the two different assimilation techniques are applied for different setups according to Tab. 1. Similar to Nakayama and Takemi (2020) a nudging zone is introduced from $x = 2.5 - 3.5$ km over the whole lateral and vertical span in the computational domain with the coarse grid spacing. An idealized target wind profile with a power-law exponent of $n = 0.25$ is assumed following the example of Nakayama and Takemi (2020). For the simulations with the fine grid spacing the nudging area is situated from $x = 0.5 - 1.5$ km in order to have enough space between the nudging zone and the horizontal outflow boundary at $x = 3$ km for the investigation of the flow. In the SBL the nudging zone ranges from $x = 2.0 - 3.0$ km.

3 Validation of the implemented Assimilation Method

In the first part of this section the results of the Newtonian relaxation method (Eq. 4) in N1 are shortly presented. In the second part the numerical results with the application of the assimilation method using the vibration equation (Eq. 5) in V1 are shown. The results of the two implemented methods are compared to the investigations of Nakayama and Takemi (2020). According to the computational setup in Nakayama and Takemi (2020) the basic turbulent boundary layer flow P1 is generated (cf. Sect. 2.4). For the nudging zone a target wind profile with an exponent of $n = 0.25$ is assumed. The spanwise velocity is approximately zero in the precursor simulation and is not changed in the nudging zone. In general, the compared simulations are in good accordance to the findings of Nakayama and Takemi (2020).

https://doi.org/10.5194/wes-2024-12
Preprint. Discussion started: 13 February 2024

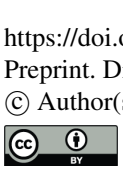

eawe european academy of wind energy
Open Access WIND ENERGY SCIENCE DISCUSSIONS

Name	Precursor Simulation	Assimilation method	Grid Resolution	Target Profile
N1	P1	Newton	coarse	idealized n=0.25
V1	P1	Vibration	coarse	idealized n=0.25
N2	P2	Newton	fine	idealized n=0.25
V2	P2	Vibration	fine	idealized n=0.25
VO	P2	Vibration	fine	observation
SO	P3	Vibration	fine	observation
SOW	P3	Vibration	fine	observation + wind turbine

Table 1. Simulations conducted in this study.

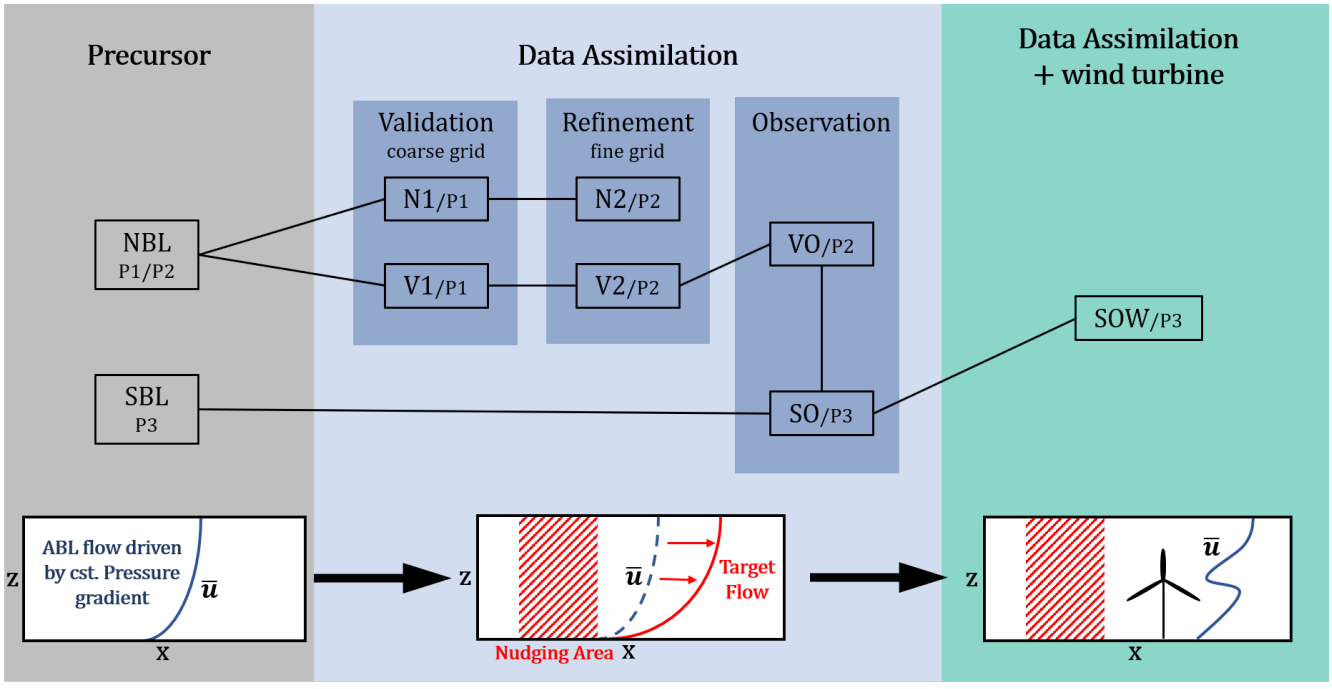

Figure 1. Schematic illustration of the different simulations considered in this study. The abbreviations indicate the simulation type following Table 1.

3.1 Results of the Newtonian Relaxation Method

In the first part of this section the results of the Newtonian relaxation method in N1 are shortly presented. The Newtonian relaxation technique is used to calculate the forcing towards the target velocity profile. As described in section 2.2, the forcing acts from 2.5 km to 3.5 km in the streamwise direction and drives the velocity towards the desired wind profile. Figure 2 shows

https://doi.org/10.5194/wes-2024-12
Preprint. Discussion started: 13 February 2024

eawe european academy of wind energy
Open Access WIND ENERGY SCIENCE DISCUSSIONS

the streamwise mean velocity $\overline{u}$ over the height for different relaxation times inside the nudging zone in a) (2.5-3.5 km) and behind the nudging zone in b) (4-5 km) averaged over the last 20 min of the simulation. The black line refers to the upstream atmospheric flow and the gray dotted line shows the target wind profile. The forcing towards the target profile is clearly visible. For a smaller relaxation time $\tau = 30$ s the amplitude of the forcing is larger and therefore the velocity is better adjusted to the target profile. For $\tau = 30$ s and $\tau = 60$ s an overestimation is apparent behind the nudging zone and the velocity tends back to its original state. The mean velocity is only slightly changed for the relaxation time $\tau = 300$ s. The results are comparable to Fig. 4 in Nakayama and Takemi (2020) and the same dependence on τ is seen.

The lower panels of Fig. 2 show the streamwise turbulence intensity (TI) which is compared for the different simulations. The TI is set in relation to data of Engineering Science Data Unit (ESDU) 85020 which provides turbulence characteristics of a neutrally stratified ABL related to a smooth surface roughness (cf. Nakayama and Takemi (2020)). Inside the nudging domain a strong decay of the turbulence intensity is perceived for a small relaxation time compared to the atmospheric flow in the precursor simulation. Only 35% of the turbulence intensity is preserved at a height of $z = 200$ m which is within the rotor area of modern wind turbines. Downstream of the nudging area the TIs have recovered well in these simulations. The results for the Newtonian Relaxation method in Nakayama and Takemi (2020) (Fig. 4) and in this study are similar for higher relaxation time scales. For small time scales, the numerical simulation with EULAG leads to a faster returning to the original turbulence intensity downstream of the nudging area than the code LOHDIM-LES developed by Nakayama et al. (2012, 2014, 2016). We assume that the differences for the TI regarding small relaxation time scales are due to different implementations of the advection scheme and surface parametrization. It can be confirmed that the main drawback of the Newtonian relaxation method Eq. 4 is the decrease of turbulence intensity when the streamwise velocity is assimilated towards the prescribed target wind profile. But in this case with a coarse grid the TI returns to the state of the upstream flow.

3.2 Results of the Assimilation Method using the Vibration Equation

The assimilation method using the vibration equation was implemented in EULAG and tested for different angular frequencies $\omega_0 = 2\pi f_0$ in order to investigate the influence of the method on the flow calculated in EULAG and to validate it with the results of Nakayama and Takemi (2020). They mentioned that f_0 must have a value smaller than the frequency of the peak in the energy spectrum in order to prevent damping of the turbulent fluctuations. Figure 3 a) and b) shows the time-averaged streamwise mean wind velocities for different values of the frequency f_0. Inside the nudging area the mean velocity is well adjusted to the target wind profile for all tested frequencies (Fig. 3a). Behind the nudging zone a small tendency towards the original wind profile can be found for all three cases (Fig. 3b). This effect can be seen as well in Fig. 8 in Nakayama and Takemi (2020). A difference is that in the LES with EULAG the mean velocities are nudged better towards the target profile for smaller frequencies. For $f_0 = 0.005$ s^{-1} at $z = 100$ m and $x = 3$ km the offset of the mean velocity to the target value is about 1 m s^{-1} in Fig. 8 in Nakayama and Takemi (2020) while the velocity is fully nudged to the target value in EULAG (Fig. 3a).

Regarding the streamwise TI in Fig. 3c a small increase can be seen in the lower 200 m inside the nudging area. Apparently, a smaller frequency leads to a higher increase of the TI. Further downstream from $x = 4 - 5$ km the turbulence intensity is

https://doi.org/10.5194/wes-2024-12
Preprint. Discussion started: 13 February 2024

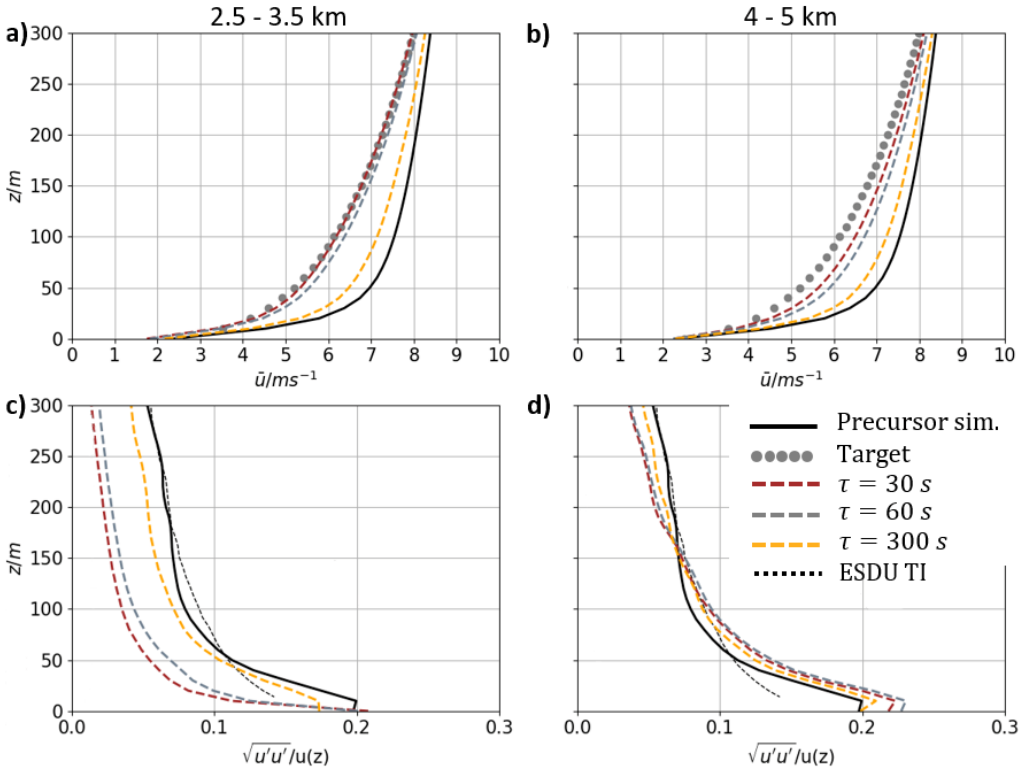

Figure 2. Results for the simulations in N1 averaged over the last 20 min. Vertical profiles of the streamwise mean velocities in a) and b) and the streamwise TI in c) and d) for different relaxation times τ inside the nudging area (2.5-3.5 km, left column) and downstream of the nudging area (4-5 km, right column). The black solid line shows the quantities for the upstream zone from 0-2 km. The gray dotted line in a) and b) presents the target wind profile. The red (gray, orange) line refers to the relaxation times $\tau = 30$ s ($\tau = 60$ s, $\tau = 300$ s). The black thin dashed line in c) and d) shows the reference TI from the ESDU 85020 data for a smooth surface.

still slightly augmented but follows in general the curve of the upstream atmospheric flow. The TI is again set in relation to data of Engineering Science Data Unit (ESDU) 85020 for a smooth surface. In the reference case from Fig. 9 in Nakayama and Takemi (2020) the TI is a little bit smaller near to the ground and higher above 150 m. The deviation near the ground results from the different modelling of the surface while in the upper layers of the atmosphere the TI is already higher in the precursor simulation of the reference case. Concerning the Reynolds stress $u'w'$ (Fig. 3e) there is also a little elevation inside the nudging zone which continues further downstream (Fig. 3f). In general it can be stated that for the tested frequencies the turbulent motions are maintained throughout the computational domain and the equilibrium state is not disturbed.

https://doi.org/10.5194/wes-2024-12
Preprint. Discussion started: 13 February 2024

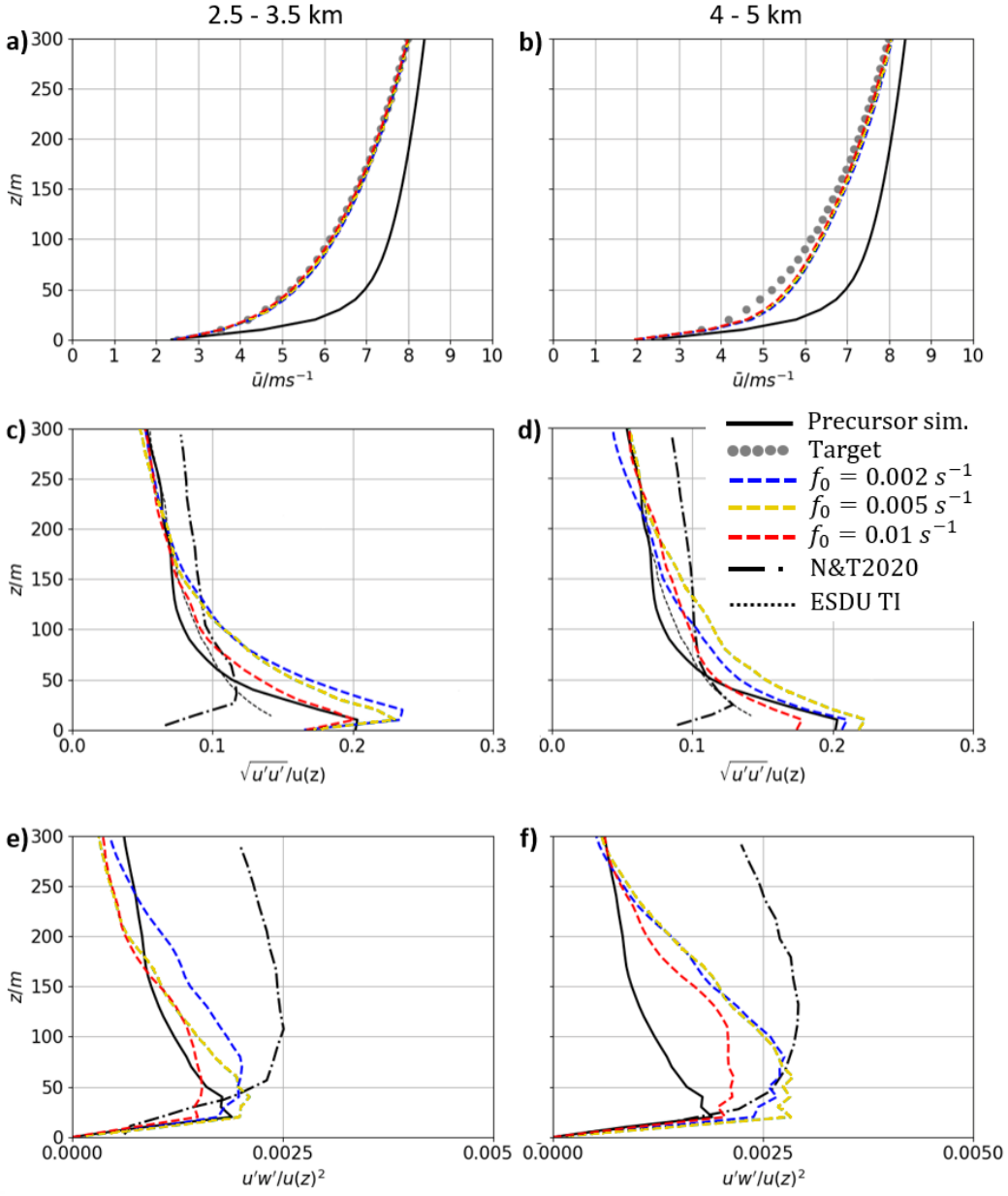

Figure 3. Results for the simulations in V1 averaged over the last 20 min. Vertical profiles of the streamwise mean velocities in a) b), the streamwise TI in c) d) and the Reynolds stress in e) f) for different frequencies f_0 inside the nudging area (2.5-3.5 km, left column) and behind the nudging area (4-5 km, right column). The black solid line shows in all graphs the quantities for the upstream zone from 0-2 km. The gray dotted line in a) and b) shows the target wind profile. The blue (green, red) lines refer to the results for the frequency $f_0 = 0.002$ s^{-1} ($f_0 = 0.005$ s^{-1}, $f_0 = 0.01$ s^{-1}). The dashed dotted line shows the reference case for $f_0 = 0.005$ s^{-1} from Nakayama and Takemi (2020). The black thin dashed line in c) and d) shows the reference TI from the ESDU 85020 data for a smooth surface.

https://doi.org/10.5194/wes-2024-12
Preprint. Discussion started: 13 February 2024

eawe european academy of wind energy
Open Access WIND ENERGY SCIENCE DISCUSSIONS

4 Data Assimilation within high resolved idealized Simulations

For wind energy purposes LESs need a higher resolution in order to calculate the forcing of the rotor blades on the flow. The assimilation methods have been tested and validated in the previous section for a coarse grid of $dx = dy = 40$ m and $dz = 10$ m (N1 and V1 in Fig. 1). Now the methods shall be tested for the high resolved simulations with a grid-spacing of $dx = dy = dz = 5$ m (N2 and V2 in Fig. 1), which is commonly used in wind-turbine LESs (cf. Vollmer et al. (2016), Englberger and Dörnbrack (2018), Chanprasert et al. (2022)).

4.1 Newtonian Assimilation

First, we consider the Newtonian assimilation method and quantify the differences between the simulations N1 with coarse grid and N2 with finer grid. In Fig. 4 a) and b) the time-averaged mean streamwise velocity profiles are shown. Inside the nudging area the mean velocity for a forcing with a small relaxation time $\tau = 30$ s is nudged even closer to the target profile in comparison to the simulation N1 (Fig. 2a). For the higher relaxation time there are no significant changes. The results for the relaxation time $\tau = 60$ s lie in between the curves for $\tau = 30$ s and $\tau = 300$ s and are not considered in the following. Apparently, with the Newtonian relaxation method the velocity can be nudged even better towards the target profile on the fine grid than on the coarse grid.

Regarding the streamwise TIs in Fig. 4 c) and d) it can be seen that the intensity is more strongly diminished in the nudging zone for $\tau = 30$ s than in the case with coarse grid and only 15% at 200 m is preserved. In the case with a larger relaxation time there is only little decrease of the TI similar to the simulation N1 (Fig. 2c and d). While the intensity recovered in the simulation N1 downstream of the nudging area this is not the case for N2. Only in the lower layers of the atmosphere up to a height of $z = 60$ m the intensity level of the upstream flow is reached. At $z = 200$ m only 40% of the upstream TI is preserved. Compared to the coarse grid the turbulence intensity couldn't be recovered to the same extent in the fine grid.
With the fine grid spacing which is necessary for wind-turbine wake simulations it is therefore crucial that the impact of the nudging method on the turbulence intensity is limited to a minimum. Once turbulence is destroyed in the atmosphere it can't be recovered to the same extent because only near-surface shear can produce turbulence in the neutral boundary layer.

4.2 Vibration Assimilation

Similarly, the simulations with a refined grid are conducted with application of the assimilation technique using the vibration equation (cf. V2 in Fig. 1). The analysis of the time-averaged streamwise mean velocity, the TI and the Reynolds stress $u'w'$ is shown in Fig. 5. The results $f_0 = 0.005$ s^{-1} lie in between the curves for $f_0 = 0.002$ s^{-1} and $f_0 = 0.01$ s^{-1} are not taken into account for the following considerations. For all frequencies the mean velocity is well adapted to the target profile (Fig. 5a). Downstream of the nudging area the velocity increases in both cases in the lower part of the atmosphere near the surface but still matches well with the target velocity profile (Fig. 5b). Regarding the streamwise TI (Fig. 5c) a decrease of the TI can be seen in the nudging zone for both cases above $z = 100$ m which is stronger for the higher frequency. Beneath $z = 100$ m the

https://doi.org/10.5194/wes-2024-12
Preprint. Discussion started: 13 February 2024

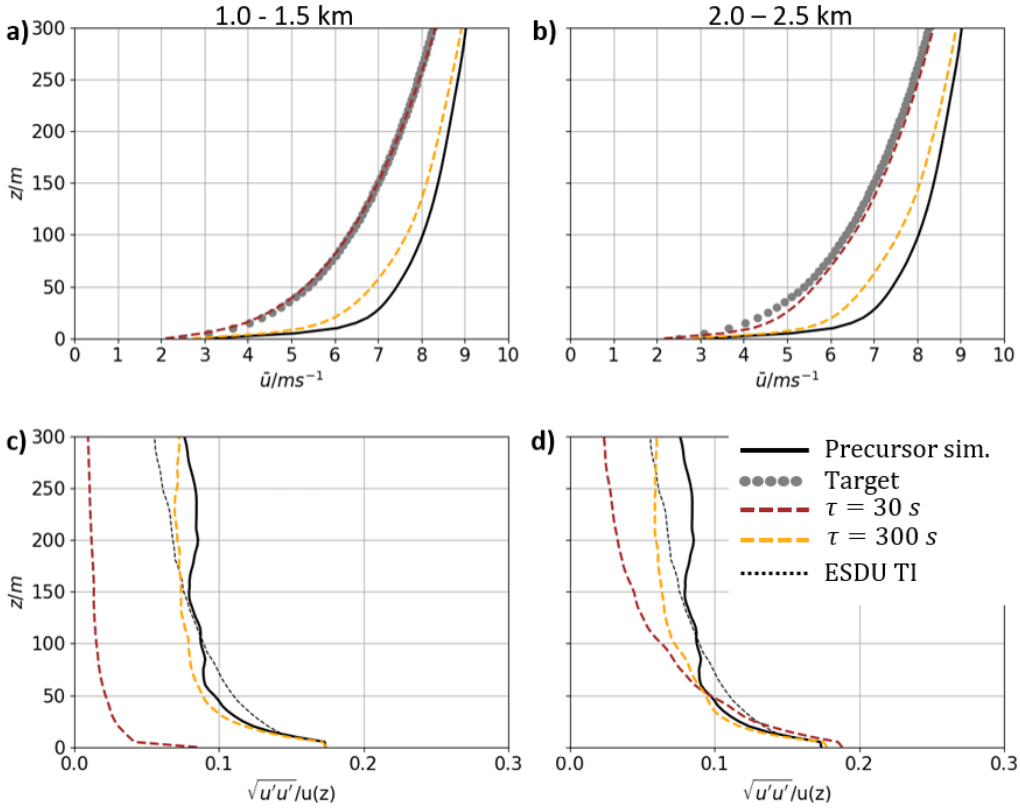

Figure 4. Results for the simulations in N2 with Newtonian assimilation technique and fine grid resolution averaged over the last 20 min. Vertical profiles of the streamwise mean velocities in a) b) and the streamwise TI in c) d) inside the nudging area (1.0-1.5 km, left column) and behind the nudging area (2.0-2.5 km, right column). The black solid line shows in all graphs the quantities for the upstream zone from 0-0.5 km. The gray dotted line in a) and b) shows the target wind profile. The brown (orange) lines refer to the results for the simulations with $\tau = 30$ s ($\tau = 300$ s) . The black thin dashed line in c) and d) shows the reference TI from the ESDU 85020 data for a smooth surface.

TI is slightly increased for $f_0 = 0.002$ s^{-1} and remains close to the original TI for the higher frequency. Behind the nudging domain (Fig. 5d) the TI is similar to the original profile below $z = 100$ m in both cases and recovers slightly above $z = 100$ m for $f_0 = 0.002$ s^{-1}. For the higher frequency of $f_0 = 0.01$ s^{-1} the TI did not recover, it even diminishes further down to 40% at $z = 200$ m . It can be concluded that a higher frequency in the assimilation method suppresses the TI more than a smaller frequency. This is in agreement with the findings of Nakayama and Takemi (2020) (cf. Fig. 9).

The mean velocity is adjusted accurately to the target profile for both frequencies. Compared to the simulations with a coarse grid V1 (Fig. 3c and d) the TI is diminished and not increased. Concerning the Reynolds stress $u'w'$ in Fig. 5f an increase of max. 90% can be observed at $z = 50$ m behind the nudging zone compared to 100% at $z = 60$ m in Fig. 3f. At $z = 200$ m there is a max. decrease of 50% in Fig. 5f and an increase of 76% in Fig. 3f. Turbulent fluctuations are damped more in higher layers of the atmosphere in the simulations with the fine grid.

https://doi.org/10.5194/wes-2024-12
Preprint. Discussion started: 13 February 2024

It can be concluded that the performance of the assimilation method with the vibration equation is more suitable for the finer grid spacing. When a target profile is assimilated with the Newtonian relaxation method a substantial decrease of the TI must be accepted. Indeed, the assimilation methods have a different impact on the atmospheric flow when the grid spacing is finer. While the mean velocity can be assimilated to the same extent, the TI is more effectively reduced for the simulations with finer spacing. This effect can be reduced when the assimilation method with the vibration equation is used. With $f_0 = 0.002$ s^{-1} the TI is decreased but is still in the proximity of the ESDU reference profile. Consequently, it is recommended for wind-turbine simulations to work with the assimilation technique using the vibration equation following Nakayama and Takemi (2020) because of the smaller impact on the atmospheric turbulence.

5 Assimilation towards a measured Wind Profile in Krummendeich

In this part of the study the target profile is near to a measured velocity profile for the wind-farm site at Krummendeich. DWL observations and data from a microwave radiometer have been analysed in order to search for a situation similar to a NBL near the ground. As period was chosen the 19.11.2021 18 UTC to 19 UTC which features strong wind shear near to the ground and a larger wind veer in the boundary layer. As continuous measurements are only available from $z = 60$ m up to $z = 470$ m a simulation with WRF was conducted for this period and continuous streamwise and spanwise velocity profiles were extracted. The WRF setup and the extraction of the used target profiles is described in appendix A. Figure 6a shows the velocity profiles of $\overline{u}$ and $\overline{v}$ for the idealized neutral precursor simulation P2 in comparison to the independent measured velocities and the target wind profiles which were extracted from WRF. A substantial difference is seen in the meridional mean velocities $\overline{v}$. In the precursor simulation for the NBL the meridional component of the velocity is nearly zero over the whole height, while the target profile shows positive values beneath $z = 200$ m and negative velocities above until -7 m s^{-1} at $z = 600$ m.
Figure 6b shows the temperature profile in comparison to the dry and moist adiabatic lapse rate. In the lowest 350 m the temperature profile shows a neutral stratification because the lapse rate is close to the moist adiabatic lapse rate (cf. Rohli and Li (2021)). This was the defined requirement for the selection of this atmospheric situation. However, the graph shows that the atmosphere is stably stratified above 350 m because the lapse rate is smaller than the reference lapse rate. Hence, we will first apply the assimilation method to the idealized NBL P2 (cf. Sect. 2.4) in Sect. 5.1 and afterwards to an idealized SBL (cf. P3 in Sect 2.4) in Sect. 5.2.

5.1 Neutral Boundary Layer as Precursor Simulation

As the temperature profile in Fig. 6 shows a neutral stratification beneath 350 m we use in a first approach the idealized NBL P2 described in section 2.4 as precursor simulation for the assimilation to the realistic wind profile. Here the results for the fine grid are shown with dx=dy=dz=5 m. While the offset of the space-averaged mean velocity of the precursor simulation $\overline{u}^P$ (averaged over the whole domain) to the mean of the target profile (averaged over the height of the ABL) $\overline{u}^T$ is large,

$$\overline{u}^P >> \overline{u}^T \quad or \quad \overline{u}^P << \overline{u}^T, \tag{7}$$

https://doi.org/10.5194/wes-2024-12
Preprint. Discussion started: 13 February 2024

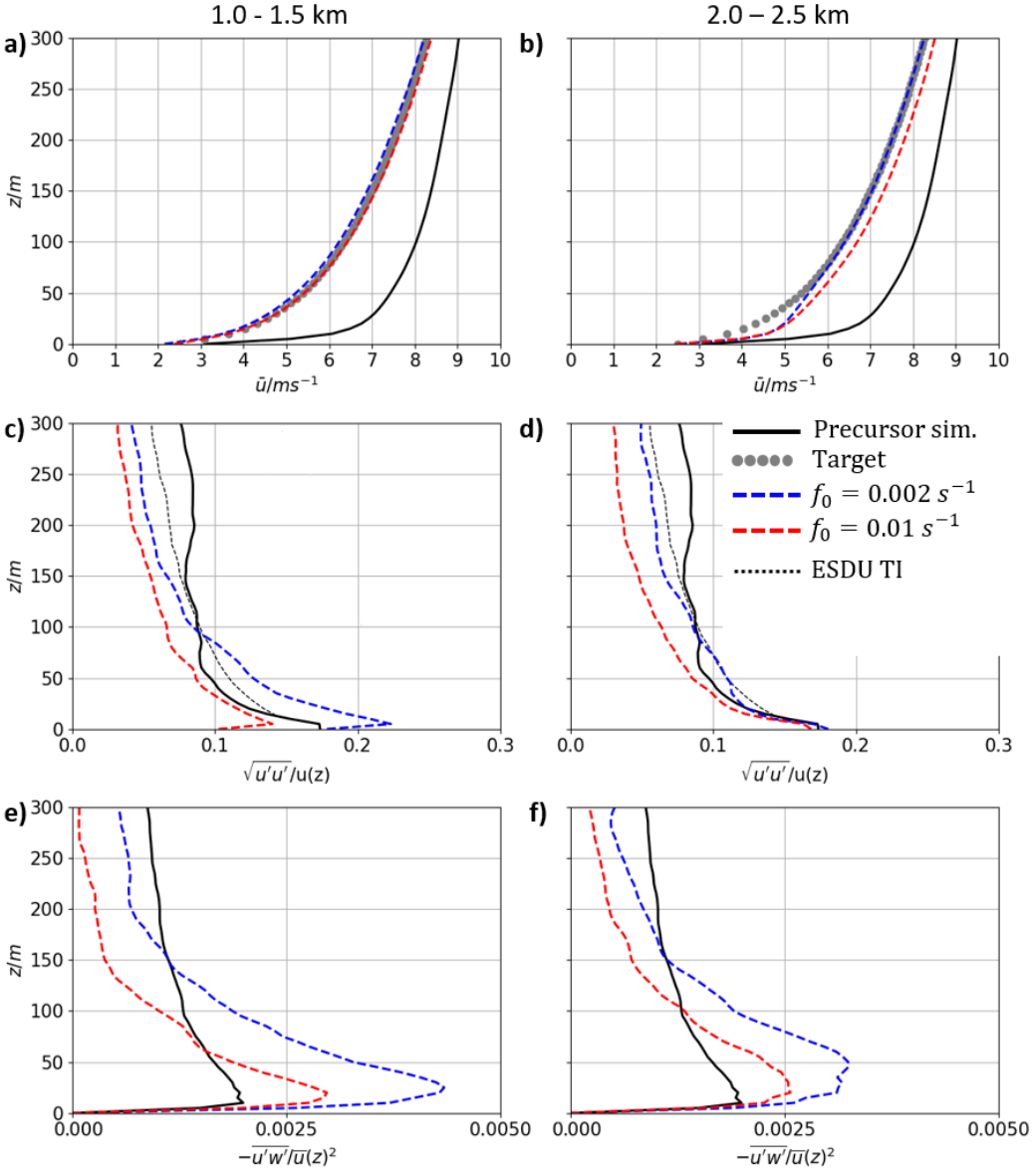

Figure 5. Results for the simulations in V2 with the vibration assimilation method and fine grid resolution averaged over the last 20 min. Vertical profiles of the streamwise mean velocities in a) b), the streamwise TI in c) d) and the Reynolds stress in e) f) for different frequencies f_0 inside the nudging area (1.0-1.5 km, left column) and behind the nudging area (2.0-2.5 km, right column). The black solid line shows in all graphs the quantities for the upstream zone from 0.0-0.5 km. The gray dotted line in a) and b) shows the target wind profile. The blue (red) lines refer to the results for the frequency $f_0 = 0.002$ s^{-1} ($f_0 = 0.01$ s^{-1}). The black thin dashed line in c) and d) shows the reference TI from the ESDU 85020 data for a smooth surface.

https://doi.org/10.5194/wes-2024-12
Preprint. Discussion started: 13 February 2024

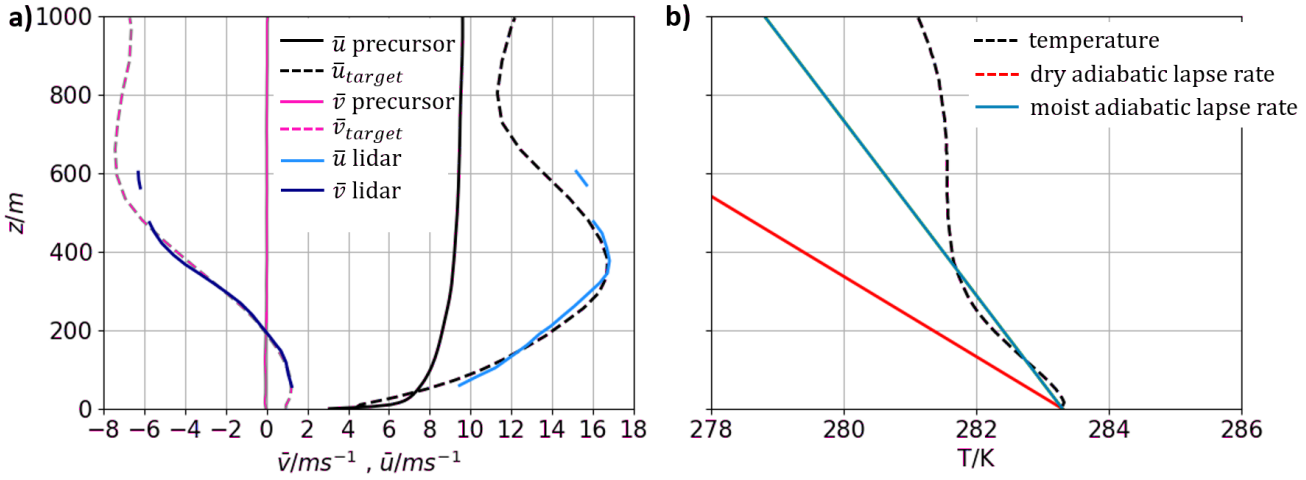

Figure 6. a) Comparison of the time-averaged mean velocities $\overline{u}$ and $\overline{v}$ of the precursor simulation for the NBL, the DWL measurements and the target velocity profiles extracted from WRF. The black (pink) solid line refers to the mean streamwise (spanwise) velocity in the precursor simulation while the black (pink) dashed line shows the streamwise (spanwise) target profile. The light blue (dark blue) line presents the observations for the streamwise (spanwise) velocity with the DWL. b) Temperature profile measured with the microwave radiometer (black dashed line) in comparison with the dry (red line) and moist (green line) adiabatic lapse rate.

the velocity at each grid point has to be changed:

$$u^{new}_{i,j,k}(z) = \alpha \overline{u}^{p}(z) + u'^{p}_{i,j,k} \tag{8}$$

with

$$\alpha = \frac{\overline{u}^{T}}{\overline{u}^{P}} \quad . \tag{9}$$

Here, $u^{new}_{i,j,k}$ is the new velocity value of the inflow field at every grid point, $\overline{u}^{p}(z)$ is the space-averaged mean value at every height of the precursor simulation and $u'^{p}_{i,j,k} = u^{p}_{i,j,k} - \overline{u}^{p}(z)$ is the fluctuation at every grid point i,j,k of the precursor simulation. This was not necessary for the investigations with the idealized profiles in Sect. 3 and Sect. 4, as the mean velocity of precursor simulation and target profile was similar. We successfully tested the assimilation method for target profiles with $\alpha = 0.67$ until $\alpha = 2$. The amplitude of the velocity fluctuations and, therefore, the TI is not changed by this adaption. For the zonal velocity profile on 19.11.2021 extracted from WRF the value $\alpha = 1.44$.

Here two different simulations (I) and (II) are shown. In the first one (I), the target velocity values are reduced (blue curves in Fig. 7):

$$u(z)^{T}_{new} = \frac{1}{\alpha} u(z)^{T} \quad with \quad \alpha = 1.44 \quad . \tag{10}$$

The second (II) was computed with the original target profile and an adapted inflow field following Eq. 8 (red curves in Fig. 7). The frequency in the vibration assimilation method was set to $f_0 = 0.002$ s^{-1} as the previous investigations showed that

https://doi.org/10.5194/wes-2024-12
Preprint. Discussion started: 13 February 2024

this value gives the best results. The vibration assimilation method was able to nudge the streamwise velocity towards the target wind profile in both cases. In the lowest 50 m an increase of $0.4 - 0.6$ m s^{-1} can be seen behind the nudging area from $2.0 - 2.5$ km as well as a small underestimation of $0.2 - 0.5$ m s^{-1} between $z = 300$ m and $z = 500$ m (Fig. 7a). Regarding the mean spanwise velocity it was not possible to nudge towards the strong negative values because the Courant-Friedrich-Lewy-criterion was violated during computation. We kept the original profile up to a height of $z = 200$ m as wind turbines usually operate in the lowest layer of the atmosphere. Above $z = 200$ m the spanwise velocity of the target profile in Fig. 6a has been reduced to the profile in Fig. 7b. Inside the nudging zone there is an exact assimilation towards the target profile with an offset less than 5% in the WT region and a slightly larger offset of 10% above 600m. Downstream of the nudging area the velocity strongly tends to the upstream state above $z = 200$ m (Fig. 7b). For the simulation (II) the spanwise mean velocity continues to be overestimated behind the nudging zone below 200 m. The streamwise TIs show an increase in both cases below $z = 100$ m and a decrease above (Fig. 7c). In the nudging area at $z = 200$ m only 45% of the TI is preserved in case (II) and 60% in case (I). Downstream of the nudging area the streamwise TI recovers and reaches even higher values than in the precursor simulation. The spanwise TI increases in both cases up to a height of $z = 300$ m and does not change considerably regarding the nudging zone and the flow behind the area (Fig. 7d). At $z = 100$ m the spanwise TI is doubled for the simulation (II) and 2.5 times larger for (I). Due to stronger wind shear and wind veer in the target profiles the equilibrium state of the precursor simulation is changed and more turbulent kinetic energy is generated. This is the reason why an increase in the TI can be seen especially behind the nudging area. A disadvantage of the assimilation of the velocity in this idealized NBL towards the measured streamwise and spanwise velocity profiles is the strong wind veer in the target profile which does not occur in the idealized case. Apparently it is not sufficient to consider only the lowest 350 m where the temperature profile is near to the moist adiabatic lapse rate and the atmosphere is neutrally stratified (cf. Fig. 6b). As the temperature profile shows a stably stratified configuration above 350 m we will use in the next section a stably stratified precursor simulation.

5.2 Stable Boundary Layer as Precursor Simulation

As response to the limitations of the results in the previous section, we propose to use a precursor simulation of a SBL computed by Englberger and Dörnbrack (2018) which has similar $\overline{u}$- and $\overline{v}$-profiles compared to the target profiles. In this configuration wind shear and especially wind veer are present in the atmospheric flow. Figure 8 shows the mean velocities $\overline{u}$ and $\overline{v}$ of the precursor simulation for the SBL in comparison to the target velocity profile.

We expect a better performance of the assimilation method as wind veer and shear are present in the precursor simulation P3 too. In this simulation the nudging zone ranges from $x = 2.0 - 3.0$ km. The assimilated profiles for the streamwise and the spanwise mean velocity can be seen in Fig. 9 a) and b). The streamwise mean velocity has been adapted for the initialization field and the inflow velocity field according to Eq. 8. There is a very good match for $\overline{u}$ already inside the nudging area and the wind speed adjusts even more further downstream. The assimilated profile for the spanwise velocity component follows the target wind profile very well. Only between 30 m and 125 m the velocity is slightly underestimated behind the nudging area. Hence, the vibration assimilation method is capable to assimilate the streamwise and spanwise mean velocity towards the

https://doi.org/10.5194/wes-2024-12
Preprint. Discussion started: 13 February 2024

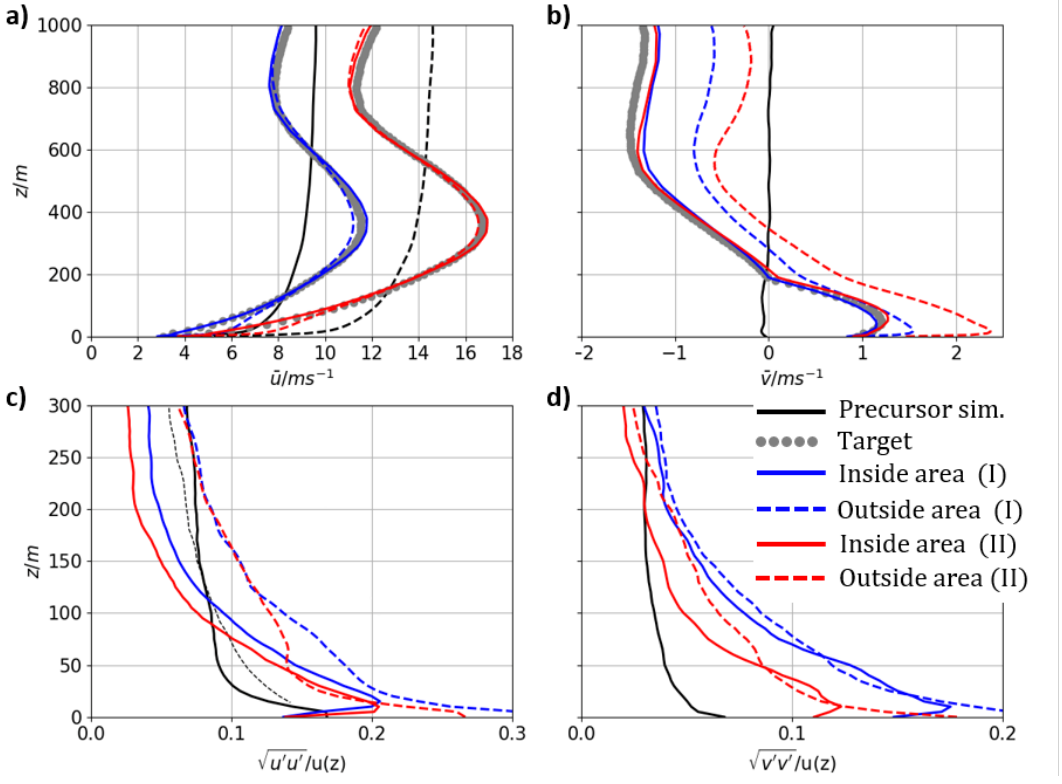

Figure 7. Results for VO of the assimilation towards measured velocity profiles with the NBL as precursor simulation and application of the vibration assimilation method averaged over the last 20 min of the simulations. The blue profiles show the results for (I) and the red profiles for (II). a) mean streamwise velocity b) mean spanwise velocity c) streamwise TI d) spanwise TI. The black solid lines refer to the upstream velocities in a) and b) and TIs in c) and d) for $x = 0 - 0.5$ km. The black dashed line in a) represents the adapted inflow field for (II). The gray dotted line in a) (b) refers to the streamwise (spanwise) target velocity profile. The colored solid (dashed) lines show the values for the frequency $f_0 = 0.002$ s^{-1} inside (behind) the nudging area from $x = 1.0 - 1.5$ km ($x = 2.0 - 2.5$ km). The black thin dashed line in c) shows the reference TI from the ESDU 85020 data for a smooth surface.

https://doi.org/10.5194/wes-2024-12
Preprint. Discussion started: 13 February 2024

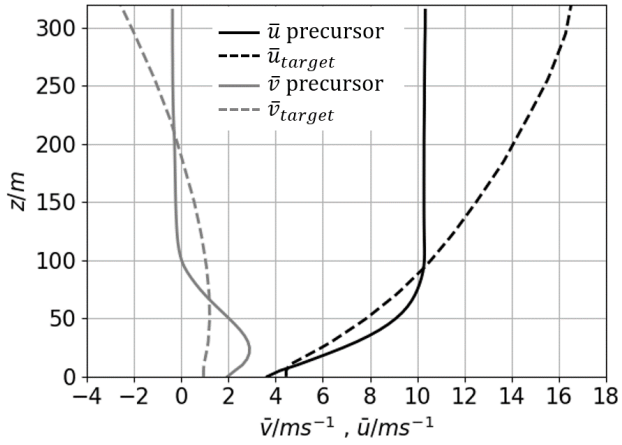

Figure 8. Comparison of the time-averaged mean velocities $\overline{u}$ and $\overline{v}$ of the precursor simulation for the SBL and the target velocity profiles. The black (gray) solid line refers to the mean streamwise (spanwise) velocity in the precursor simulation while the black (gray) dashed line shows the streamwise (spanwise) target profile.

target profiles. Compared to the assimilation in the NBL (Fig. 7) notably the spanwise velocity could be nudged towards the target profile and did not tend back to the spanwise profile of P3 downstream of the nudging zone.

Regarding the streamwise and spanwise TI in Fig. 9 c) and d) an increase is noticeable. Near to the ground the streamwise TI inside the nudging zone is over three times higher than in the SBL and over five times higher behind the zone. With growing height the TI decreases and has the same magnitude above $z = 150$ m inside the nudging zone. For $x = 3.5 - 4.5$ km the TI is still four times higher at $z = 100$ m and two times higher at $z = 250$ m. The target profile shows a velocity gradient over the whole height while shear is only present up to $z = 100$ m in the precursor simulation. The increase of the shear beneath $z = 100$ m leads significantly to a higher turbulence intensity. The spanwise TI is also about three times higher over the whole height compared to the precursor simulation (Fig. 9d). In the precursor simulation wind veer occurs only in the lowest 100 m. Above, the spanwise mean velocity $\overline{v}$ is nearly constant at $\overline{v} = -0.2$ m s^{-1}. The assimilation leads to a spanwise velocity profile where veering is present over the whole height which increases the spanwise TI.

Figure 10 gives an overview of the results for the considered precursor simulations with the application of the vibration assimilation method. It can be concluded, that the wind profiles of the SBL are better suited for the assimilation towards the measured velocity profiles. Figure 10a and b show a good accord of the velocities in the SBL downstream to the nudging zone. Especially the gap between the assimilated spanwise velocity profile for the NBL and the target profile is striking (Fig. 10b). Indeed, the TIs in Fig. 10c and d for the NBL are closer to the DWL-measurements and the reference data from WRF (resolved TI) than for the SBL. With the SBL as precursor simulation the TIs are changed due to the assimilation method to a higher intensity than in the precursor simulation. However, there might be mesoscale effects which are not taken into account by the assimilation method and the precursor simulation.

https://doi.org/10.5194/wes-2024-12
Preprint. Discussion started: 13 February 2024

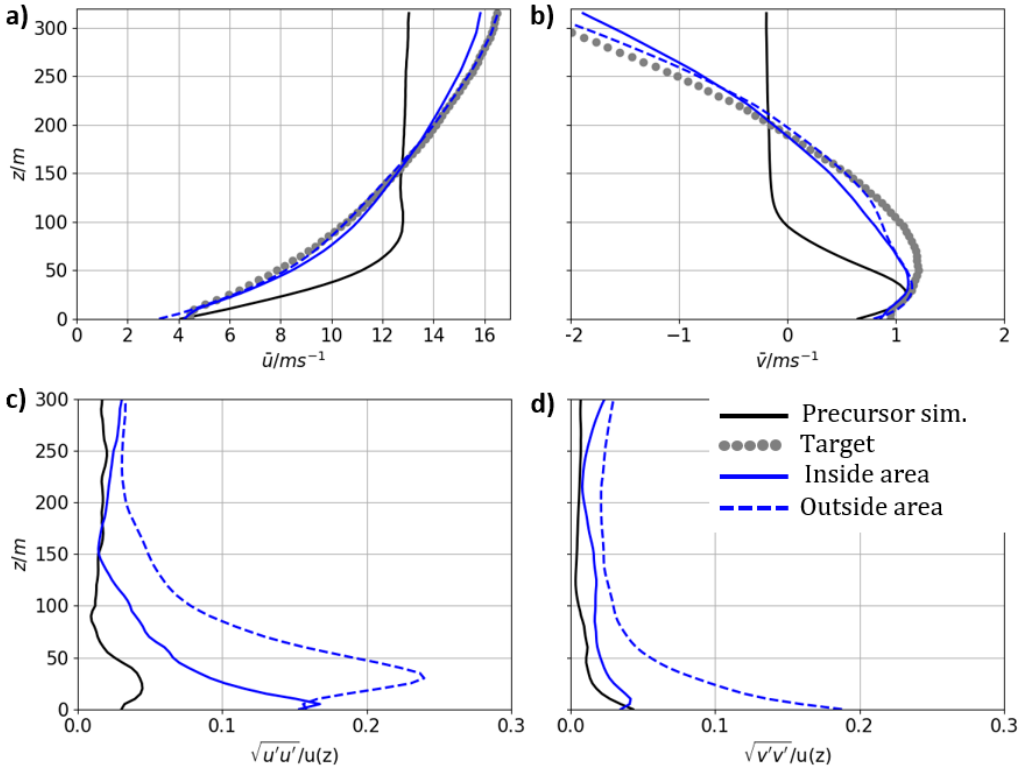

Figure 9. Results for SO of the assimilation towards the measured boundary layer profile with a SBL as precursor simulation and application of the vibration assimilation method averaged over the last 20 min of the simulation. a) mean streamwise velocity b) mean spanwise velocity c) streamwise TI d) spanwise TI. The black solid lines refer to the upstream velocities in a) and b) and TIs in c) and d) for $x = 0 - 2$ km. The gray dotted line in a) (b)) refers to the streamwise (spanwise) target velocity profile. The blue solid (dashed) lines show the values for the frequency $f_0 = 0.002$ s^{-1} inside (behind) the nudging area from $x = 2.0 - 3.0$ km ($x = 3.5 - 4.5$ km).

6 Analysis of the Wind-Turbine Wake for an assimilated Atmospheric Inflow

In this section the assimilation of a precursor simulation towards the realistic wind profiles shall be combined with the simulation of the wake behind a wind turbine. Therefore, the assimilated SBL of section 5.2 is considered as the vibration assimilation method showed the best performance regarding mean velocity profiles. Behind the nudging zone the wind turbine is modeled in EULAG according to the parametrization presented in section 2.1. The nudging area is located at $x = 0.3 - 1.3$ km and the rotor is placed 200 m behind the nudging zone at $x = 1.5$ km. The computational domain for the wake analysis has a length of 3620 m which is sufficient for the investigations until $22D = 2772$ m behind the rotor. First, we conducted one simulation with the wind turbine and the original SBL as a reference case. In a second simulation the inflow of the SBL is assimilated by the vibration assimilation method towards the measured target wind profile from Sect. 5.2. The wake of the wind turbine

https://doi.org/10.5194/wes-2024-12
Preprint. Discussion started: 13 February 2024

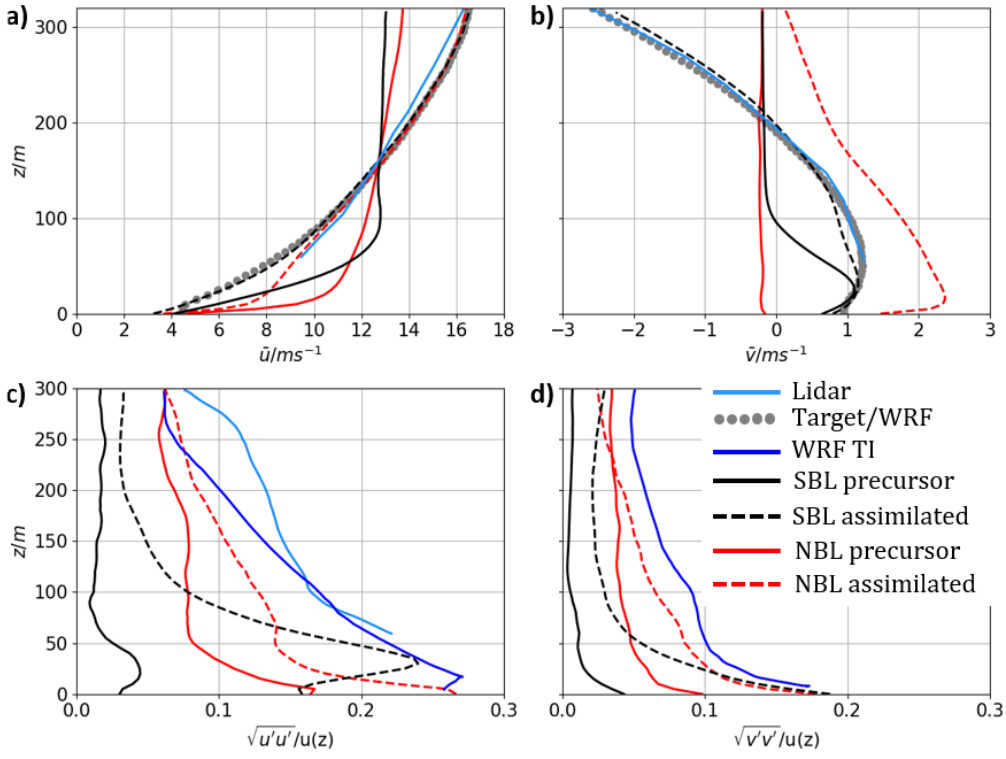

Figure 10. Comparison of the a) mean streamwise velocity b) mean spanwise velocity c) streamwise TI and d) spanwise TI for the two different precursor simulations and DWL- and WRF-data averaged over the last 20 min of the simulations. The black (red) lines refer to simulation with a SBL (NBL) as precursor simulation. The solid (dashed) line shows the curves upstream (downstream) to the nudging zone. The gray dotted line in a) (b)) refers to the streamwise (spanwise) target velocity profile out of WRF. The light blue line in a) (b)) shows the DWL-data for the streamwise (spanwise) velocity and in c) the streamwise TI. The dark blue line in c) (d)) shows the streamwise (spanwise) TI calculated from the WRF flow field.

is computed for a rotor plane which is at hub height orthogonal to the main wind direction. The time-averaged streamwise velocity component for both cases is shown for three x - y planes in Fig. 11. The influence of the assimilation method on the mean streamwise velocity is clearly visible at hub height (Fig. 11e) and in the lower part of the rotor (Fig. 11f). The velocities are reduced towards the slower target wind profile. As the rotor plane is turned towards the main wind direction, the influence
415 of the changed wind veer is visible in Fig. 11d where the wake is slightly deflected southwards because of a negative spanwise velocity. Also in Fig. 11f a small deflection of the far wake to the north is seen due to the positive spanwise wind speed below the nacelle. The small asymmetry in the near wake in Fig. 11d (f) can be explained by the negative (positive) spanwise velocity above (beneath) the nacelle and the induced flow due to the rotation of the rotor. Furthermore, the streamwise wake extension is decreased for the case with assimilation. For the reference case a velocity deficit ($VD_{i,j,k} \equiv \frac{\overline{u_{1,j,k}} - \overline{u_{i,j,k}}}{\overline{u_{1,j,k}}}$) of 10% is seen at
420 $x = 22D$ behind the rotor at hub height and at $x = 20D$ the deficit reaches a value of 20% (Fig. 11b). In the simulations with

https://doi.org/10.5194/wes-2024-12
Preprint. Discussion started: 13 February 2024

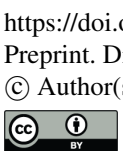

eawe european academy of wind energy
Open Access WIND ENERGY SCIENCE DISCUSSIONS

vibration assimilation a deficit of 10% (20%) is seen at $x = 20D$ ($x = 14D$) at hub height (Fig. 11e). Also above and beneath hub height the streamwise wake extension is reduced for the simulations with the assimilation method (Fig. 11d and f). One reason for the reduced wake extension is the lower streamwise wind speed of the assimilated inflow. Another finding is that the turbulence in the wake is higher when the assimilation method is applied. We have already shown in Sect. 5.2 that the TI is increased behind the nudging area due to stronger shear and veer in the atmosphere. It is therefore consistent that the turbulence is also higher behind the wind turbine. This effect leads to a more rapid recovery of the wake behind the wind turbine. This effect has already been observed by Englberger and Dörnbrack (2018).

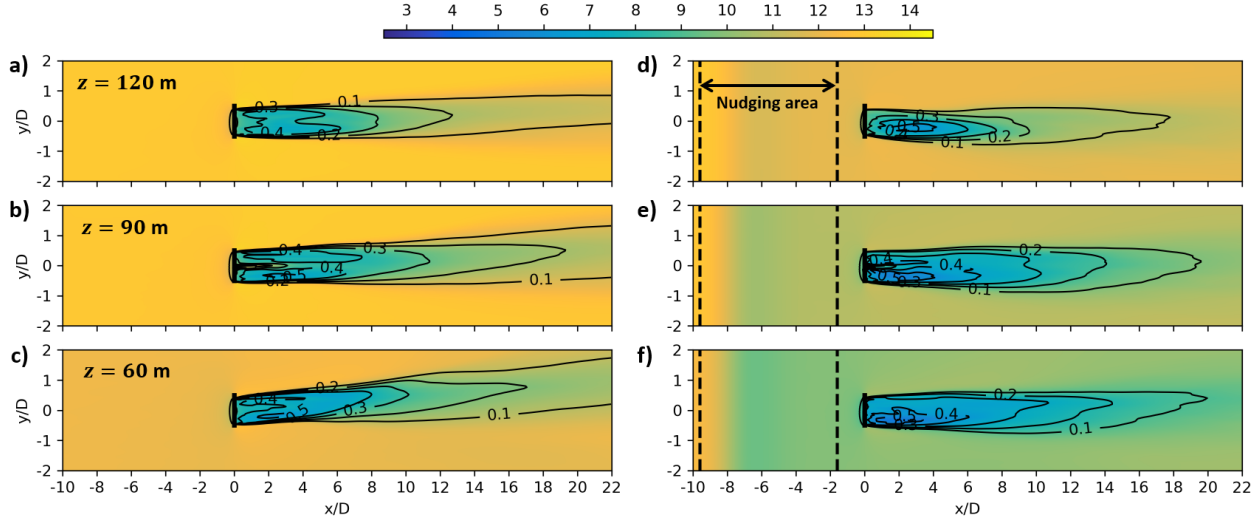

Figure 11. Coloured contours of the time-averaged streamwise velocity component $\overline{u_{i,j,k}}$ in m s^{-1} without data assimilation in a), b) and c) and with vibration assimilation in d), e) and f) averaged over 20 min at the end of the simulation. b) and e) show the x - y plane at hub height $z = 90$ m. a) and d) (c)and f)) correspond to the x - y planes at $Z = 90m + R/2 = 120$ m ($Z = 90m - R/2 = 60$ m). The black contours represent the velocity deficit $VD_{i,j,k}$ at the same vertical location calculated in relation to the upstream velocity at $x = -200$ m. The axes are normalized by the rotor diameter $D = 126$ m, whereby $x/D = 0$ indicates the position of the rotor.

Figure 12a and c show the lateral view on a vertical plane through the center of the wind turbine with the visualization of the time-averaged streamwise velocity component $\overline{u}$. The figure shows that the velocity deficit in the wake is very similar for both simulations in the proximity of the rotor until $x < 10D$. Further downstream the reduced wake extension is seen for the simulation with assimilation of the velocities (Fig. 12c). Figures 11 and 12 show the interaction of the wake behind the rotor with a stable atmospheric boundary layer flow. The results for both simulations are in good accordance to other studies from Bhaganagar and Debnath (2014), Abkar and Porté-Agel (2015) and Englberger and Dörnbrack (2018) who considered wind-turbine wakes in SBLs. The applied assimilation method changes wind veer and shear in the atmospheric flow. The changed wake structure can also be seen in a downstream view at $x = 5D$ in Fig. 12b and d. While the spanwise wind speed was

https://doi.org/10.5194/wes-2024-12
Preprint. Discussion started: 13 February 2024

eawe european academy of wind energy
Open Access WIND ENERGY SCIENCE DISCUSSIONS

predominant in the lower section of the rotor in the reference case (Fig. 12b) the assimilated wind veer leads to a deflection of the wake for $z > z_{hub}$ (Fig. 12d).

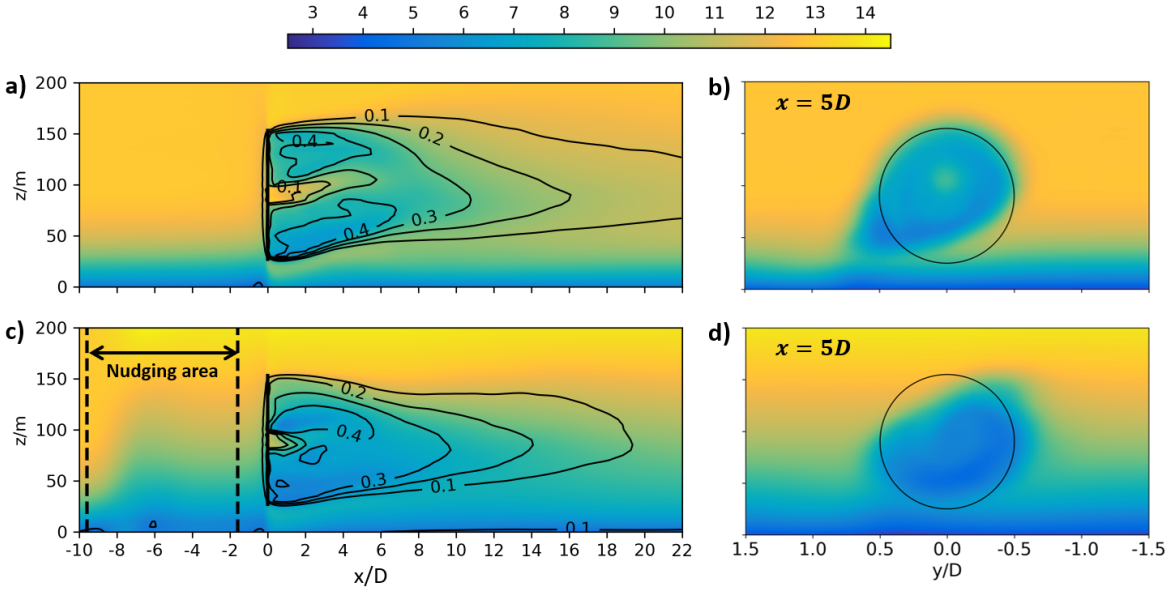

Figure 12. Coloured contours of the time-averaged streamwise velocity component $\overline{u_{i,j_0,k}}$ in m s^{-1} without assimilation in a) and b) and with vibration assimilation in c) and d) averaged over 20 min at the end of the simulation. In a) and c) the vertical x - z plane at the position $y = 0$ perpendicular to the turbine is presented. The black contours represent the velocity deficit $VD_{i,j_0,k}$ at the same spanwise location calculated in relation to the upstream velocity at $x = -200$ m. The abscissa is divided by the diameter of the rotor, whereby $x/D = 0$ indicates the position of the rotor. b) and d) show streamwise velocity component at a downward position of x=5D. The black circles represent the rotor area.

The streamwise TI is shown in Fig. 13 for different distances upstream and downstream of the rotor normalized by the mean streamwise velocity at hub height. The influence of the assimilation method can be seen comparing the plots for the distances $x/D = -10$ and $x/D = -1$ as the TI is increased behind the nudging zone. For the analysis of the downstream regions in the simulation with assimilation the TI at the position $x/D = -1$ is subtracted in order to separate the TI induced by the rotor from the TI induced by the assimilation method. At hub height and above the hub an increase of the streamwise TI can be seen in the near wake until $x/D \leq 3$ for the case with nudging. In the reference case the intensity increases slightly over the whole rotor. The TI for $5 \leq x/D \leq 10$ increases further for the reference case over the whole rotor area. In the simulation with nudging the TI beneath hub height is very similar to the TI in the reference case but it is about two times higher above the hub. For a distance of $x/D = 20$ the TI decreases in the simulation with data assimilation as the wake already dissolves. In the far wake for $x/D > 10$ the TIs match very well for the two simulations. The elevated TI in the nudging simulation until $x/D = 10$ leads to the more rapidly recovery of the wake behind the wind turbine which were seen in Fig. 11 and 12c.

https://doi.org/10.5194/wes-2024-12
Preprint. Discussion started: 13 February 2024

eawe european academy of wind energy
Open Access WIND ENERGY SCIENCE DISCUSSIONS

Currently, there is no measurement data available for wakes behind the wind turbines at the wind-farm site at Krummendeich. Therefore, no quantitative analysis of the wake which is shown in this study could be done at this point. The characteristics of the wake in the near stably stratified boundary layer are accordingly to comparable studies in the literature. The differences in the wake compared to the reference case without nudging can be explained by the changes in the inflow field. It has been proven in this chapter that the vibration assimilation method is capable of changing the inflow velocities towards realistic target velocity profiles for wind turbine simulations.

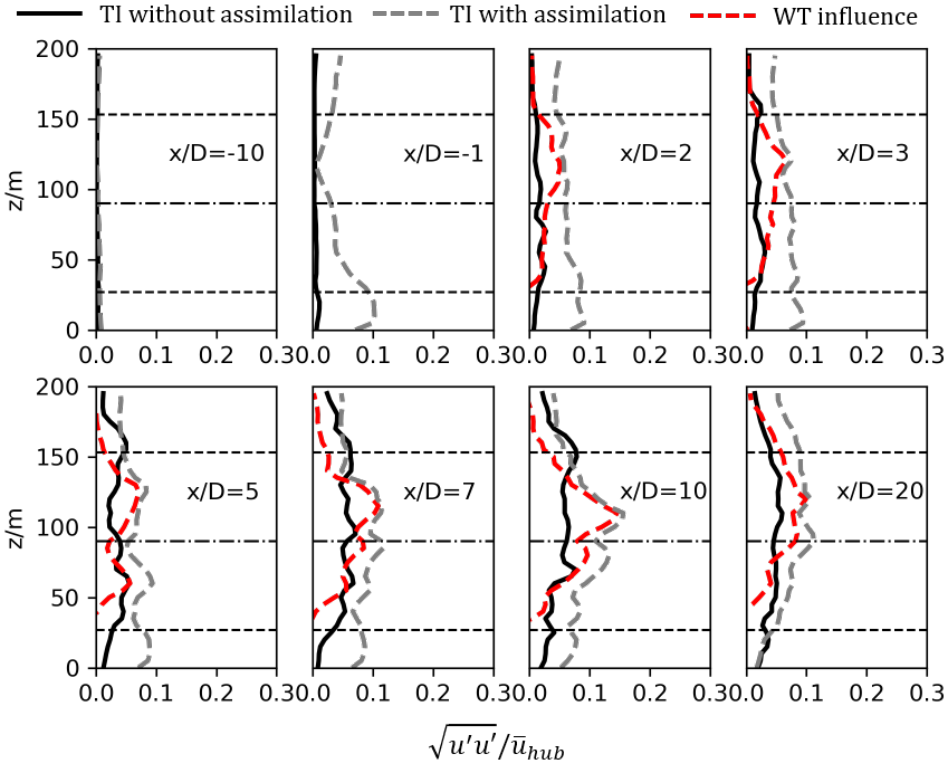

Figure 13. Comparison of vertical profiles of the streamwise turbulence intensity $\sqrt{u'u'}/\bar{u}_{hub}$ for different distances upstream and downstream of the rotor normalized by the rotor diameter $D = 126$ m. The black solid curves refer to the reference simulation without assimilation. The gray dashed lines refer to the TI in the simulation with nudging and the red dashed lines show the the TI induced by the WT (TI minus TI at x/D=-1 with assimilation). The hub height is marked with the black dashed dotted line and the top tip and bottom tip with the black dashed lines.

https://doi.org/10.5194/wes-2024-12
Preprint. Discussion started: 13 February 2024

eawe european academy of wind energy
Open Access WIND ENERGY SCIENCE DISCUSSIONS

7 Conclusions

The data assimilation technique using the vibration equation was validated for the numerical code EULAG and sensitivity studies in regard to grid refinement were conducted. The vibration assimilation method was applied to assimilate idealized precursor simulations towards measured target wind profiles for the wind farm site WiValdi at Krummendeich. This ABL with assimilated wind speeds was used as inflow for the 5MW NREL wind turbine. The developed wake and its interaction with the stably stratified boundary layer flow were investigated. The present study contributes to the efficient integration of observational data into LESs in order to generate realistic atmospheric inflow fields for wind-turbine simulations.

The comparative analysis of the implemented vibration assimilation method with the Newtonian relaxation for a coarse grid spacing has shown the differences and advantages of the new implemented method. We can now answer the question if the both relaxation methods are able to preserve turbulence in LES. The use of the Newtonian Relaxation technique is not appropriate for wind-energy purposes because of the severe decrease of atmospheric turbulence in the simulations. Especially for a fine grid the vibration assimilation method showed a better performance in regard to the atmospheric turbulence. We have found that a smaller frequency in the vibration equation leads to a lesser decrease of TI. The presented vibration assimilation method is therefore capable to assimilate the atmospheric inflow towards target profiles for wind-energy purposes.

For an efficient and robust use of the vibration assimilation technique it is necessary that a single precursor simulation can be adapted to an arbitrary target velocity profile. Hence, computational resources can be saved and long and expensive simulations which need to match anticipated characteristics in the ABL can be avoided. The vibration assimilation method changed the mean velocity profiles of the idealized precursor simulations to measured profiles for the wind-farm site WiValdi. The concurrent adaption of the TI shows that the method represents turbulence generating processes which occur when the idealized ABL is transformed into a more realistic boundary layer. The importance of the consideration of the atmospheric stratification (lapse rate) has been presented. The vibration assimilation method is only successful when the basic atmospheric stratification in the precursor simulation and the target profile agree and the main characteristics of the wind conditions match (e.g. wind veer). This study has shown that for wind-energy purposes it is not sufficient to consider only the lowest 300 m of the atmosphere but rather the whole boundary layer height. For the assimilation of velocities in atmospheric precursor simulations towards realistic wind profiles it is hence necessary, that the stratification of the atmosphere in the precursor simulation is similar to the conditions in the boundary layer in which the observations are performed.

Finally, the assimilated flow field was used as inflow for a wind turbine which is parameterized with the blade element momentum method as rotating actuator disc. The wake behind the wind turbine in the assimilated flow field showed well known structures and intensity profiles. In general, the discussed effects on the wake evoked by the nudging method are reasonable. It must be said that at the moment of the DWL-measurements at Krummendeich the wind turbines were still under construction and measurement data of the wake are not available for a comparative analysis in this study.

In conclusion, the presented vibration assimilation method can assimilate atmospheric inflow fields for wind energy purposes. Arbitrary velocity profiles for a specified atmospheric stratification can be reproduced by the developed LES model. The conditions in the precursor simulation and the target wind profiles must show similar characteristics for a successful result of the

https://doi.org/10.5194/wes-2024-12
Preprint. Discussion started: 13 February 2024

assimilation method. Further tests with different atmospheric stratifications and more observational data will be conducted and presented at the TORQUE 2024 (Wrba et al. (under review)). As soon as measurement data of the wake behind the wind turbine at the wind-farm site WiValdi is available, a comparative analysis of the computed wake in EULAG and the wake measurements is possible.

Appendix A: WRF Setup

The wind profiles used as target velocity profiles in Sect. 5 and Sect. 6 were extracted from a simulation using the WRF model version 4.4.1. A particular time period during 19.11.2021 was chosen from DWL-observations taken at the research wind farm located at Krummendeich (cf. Sect. 2.3). On this day the DWL-observations showed that the conditions at the wind park represented a quasi-neutral boundary layer with nominal wind speeds at hub height of roughly 10 m s^{-1}.

The WRF simulation consists of four nested domains, with a horizontal grid spacing of 5 km, 1 km, 200 m and 40 m for domains 1-4, respectively. The domains with sub-kilometer grid spacing are run in LES mode. Vertical nesting is applied also, so that higher vertical resolution is used in the domains with higher horizontal resolution. The mean target profiles for the streamwise and spanwise velocity used in EULAG are extracted from D4 and vertically interpolated so that there is a constant $dz = 5$ m. Initial and boundary conditions are supplied from the European Centre for Medium-Range Weather Forecasts (ECMWF) operational analyses, which has a temporal resolution of 6 h. Topography data for the LES domains are provided by the Copernicus digital elevation model and are available at a horizontal grid spacing of 90 m and 30 m. The model top was set at about 12 km height to include tropopause effects. A 3 km upper damping layer is implemented, to restrict reflection of gravity waves. The Monin-Obukhov scheme is used to simulate the surface layer (Janjic (1996)). Additionally, the Noah-MP land-surface model (Niu et al. (2011)), the Rapid Radiative Transfer Model long-wave scheme (Mlawer et al. (1997)), the Dudhia short-wave scheme (Dudhia (1989)), the WRF single-moment five-class microphysics scheme (Hong and Lim (2006)) are used. In domains 1 and 2 the Kain–Fritsch cumulus parameterization scheme is implemented (Kain and Fritsch (1990)) and a planetary boundary scheme is used, namely the Mellor–Yamada–Janjic TKE scheme (Mellor and Yamada (1982)). In the LES domains (domains 3-4) the cumulus parameterization and planetary boundary schemes are switched off, and SGS turbulence is parameterized by a three-dimensional 1.5-order TKE closure (Deardorff (1980)). The simulations were performed for a total of 7 hours, from 12 UTC to 19 UTC on 19.11.2021.

Author contributions. All authors conceived the idea. LW performed the simulations and prepared the manuscript with contributions from all co-authors. NW performed the DWL and MWR measurements and GK computed the WRF simulations.

Competing interests. The contact author has declared that neither of the authors has any competing interests.

https://doi.org/10.5194/wes-2024-12
Preprint. Discussion started: 13 February 2024

Acknowledgements. Measurements at the WiValdi research park (https://windenergy-researchfarm.com/) were conducted as part of the research project Deutsche Forschungsplattform für Windenergie (http://dfwind.de). We greatly acknowledge the financial support of the German Federal Ministry for Economic Affairs and Climate Action, through FKZ 0325936, that enabled this work.The authors gratefully acknowledge the Gauss Centre for Supercomputing e.V. (http://www.gauss-center. eu) for funding this project by providing computing time on the GCS Supercomputer SuperMUC at Leibniz Supercomputing Centre (LRZ, www.lrz.de). Funding was provided by German Aerospace Center (DLR e.V.).

https://doi.org/10.5194/wes-2024-12
Preprint. Discussion started: 13 February 2024

eawe european academy of wind energy
Open Access WIND ENERGY SCIENCE DISCUSSIONS

References

Abkar, M. and Porté-Agel, F.: Influence of atmospheric stability on wind-turbine wakes: A large-eddy simulation study, Physics of fluids, 27, 035 104, https://doi.org/https://doi.org/10.1063/1.4913695, 2015.

Abkar, M., Sharifi, A., and Porté-Agel, F.: Wake flow in a wind farm during a diurnal cycle, Journal of Turbulence, 17, 420–441, 2016.

Allaerts, D., Quon, E., Draxl, C., and Churchfield, M.: Development of a time–height profile assimilation technique for large-eddy simulation, Boundary-Layer Meteorology, 176, 329–348, 2020.

Allaerts, D., Quon, E., and Churchfield, M.: Using observational mean-flow data to drive large-eddy simulations of a diurnal cycle at the SWiFT site, Wind Energy, 26, 469–492, 2023.

Arcucci, R., D'Amore, L., Pistoia, J., Toumi, R., and Murli, A.: On the variational data assimilation problem solving and sensitivity analysis, Journal of Computational Physics, 335, 311–326, 2017.

Bhaganagar, K. and Debnath, M.: Implications of Stably Stratified Atmospheric Boundary Layer Turbulence on the Near-Wake Structure of Wind Turbines, Energies, 7, 5740–5763, https://doi.org/10.3390/en7095740, 2014.

Bhaganagar, K. and Debnath, M.: The effects of mean atmospheric forcings of the stable atmospheric boundary layer on wind turbine wake, Journal of Renewable and Sustainable Energy, 7, 013 124, https://doi.org/https://doi.org/10.1063/1.4907687, 2015.

Chanprasert, W., Sharma, R., Cater, J., and Norris, S.: Large Eddy Simulation of wind turbine wake interaction in directionally sheared inflows, Renewable Energy, 201, 1096–1110, 2022.

Deardorff, J. W.: Three-dimensional numerical study of turbulence in an entraining mixed layer, Boundary-Layer Meteorology, 7, 199–226, https://doi.org/https://doi.org/10.1007/BF00227913, 1974.

Deardorff, J. W.: Stratocumulus-capped mixed layers derived from a three-dimensional model, Boundary-layer meteorology, 18, 495–527, 1980.

Dudhia, J.: Numerical study of convection observed during the winter monsoon experiment using a mesoscale two-dimensional model, Journal of Atmospheric Sciences, 46, 3077–3107, 1989.

Elliott, J. R. and Smolarkiewicz, P. K.: Eddy resolving simulations of turbulent solar convection, International Journal for Numerical Methods in Fluids, 39, 855–864, 2002.

Englberger, A. and Dörnbrack, A.: Impact of neutral boundary-layer turbulence on wind-turbine wakes: a numerical modelling study, Boundary-Layer Meteorology, 162, 427–449, https://doi.org/https://doi.org/10.1007/s10546-016-0208-z, 2017.

Englberger, A. and Dörnbrack, A.: Impact of the Diurnal Cycle of the Atmospheric Boundary Layer on Wind-Turbine Wakes: A Numerical Modelling Study, Boundary Layer Meteorology, https://doi.org/https://doi.org/10.1007/s10546-017-0309-3, 2018.

Hansen, M.: Aerodynamics of Wind Turbines, Earthscan, https://books.google.de/books?id=GVD_HDPix6YC, 2013.

Haupt, S. E., Kosovic, B., Berg, L. K., Kaul, C. M., Churchfield, M., Mirocha, J., Allaerts, D., Brummet, T., Davis, S., DeCastro, A., et al.: Lessons learned in coupling atmospheric models across scales for onshore and offshore wind energy, Wind Energy Science Discussions, 2022, 1–36, 2022.

Heinze, R., Moseley, C., Böske, L. N., Muppa, S. K., Maurer, V., Raasch, S., and Stevens, B.: Evaluation of large-eddy simulations forced with mesoscale model output for a multi-week period during a measurement campaign, Atmospheric Chemistry and Physics, 17, 7083–7109, 2017.

Hong, S.-Y. and Lim, J.-O. J.: The WRF single-moment 6-class microphysics scheme (WSM6), Asia-Pacific Journal of Atmospheric Sciences, 42, 129–151, 2006.

https://doi.org/10.5194/wes-2024-12
Preprint. Discussion started: 13 February 2024

Janjic, Z.: The Mellor-Yamada level-2.5 scheme in the NCEP Eta model, in: Preprint, 11ˆ< th> AMS Conference on Numerical Weather Prediction, Norfolk, VA, 1996, 1996.

Jonkman, J., Butterfield, S., Musial, W., and Scott, G.: Definition of a 5-MW Reference Wind Turbine for Offshore System Development, https://doi.org/10.2172/947422, 2009.

Kain, J. S. and Fritsch, J. M.: A one-dimensional entraining/detraining plume model and its application in convective parameterization, Journal of Atmospheric Sciences, 47, 2784–2802, 1990.

Lilly, D. K.: On the computational stability of numerical solutions of time-dependent non-linear geophysical fluid dynamics problems, Monthly Weather Review, 93, 11–25, 1965.

Lu, H. and Porté-Agel, F.: Large-eddy simulation of a very large wind farm in a stable atmospheric boundary layer, Physics of Fluids, 23, 2011.

Mann, J.: The spatial structure of neutral atmospheric surface-layer turbulence, Journal of fluid mechanics, 273, 141–168, https://doi.org/https://doi.org/10.1017/S0022112094001886, 1994.

Margolin, L. G., Smolarkiewicz, P. K., and Sorbjan, Z.: Large-eddy simulations of convective boundary layers using nonoscillatory differencing, Physica D: Nonlinear Phenomena, 133, 390–397, 1999.

Maronga, B., Gryschka, M., Heinze, R., Hoffmann, F., Kanani-Sühring, F., Keck, M., Ketelsen, K., Letzel, M. O., Sühring, M., and Raasch, S.: The Parallelized Large-Eddy Simulation Model (PALM) version 4.0 for atmospheric and oceanic flows: model formulation, recent developments, and future perspectives, Geoscientific Model Development, 8, 2515–2551, 2015.

Mellor, G. L. and Yamada, T.: Development of a turbulence closure model for geophysical fluid problems, Reviews of Geophysics, 20, 851–875, 1982.

Mirocha, J., Kosovic, B., Aitken, M., and Lundquist, J.: Implementation of a generalized actuator disk wind turbine model into the weather research and forecasting model for large-eddy simulation applications, Journal of Renewable and Sustainable Energy, 6, 013 104, https://doi.org/https://doi.org/10.1063/1.4861061, 2014.

Mlawer, E. J., Taubman, S. J., Brown, P. D., Iacono, M. J., and Clough, S. A.: Radiative transfer for inhomogeneous atmospheres: RRTM, a validated correlated-k model for the longwave, Journal of Geophysical Research: Atmospheres, 102, 16 663–16 682, 1997.

Nakayama, H. and Takemi, T.: Development of a Data Assimilation Method Using Vibration Equation for Large-Eddy Simulations of Turbulent Boundary Layer Flows, Journal of Advances in Modeling Earth Systems, 12, e2019MS001 872, 2020.

Nakayama, H., Takemi, T., and Nagai, H.: Large-eddy simulation of urban boundary-layer flows by generating turbulent inflows from mesoscale meteorological simulations, Atmospheric Science Letters, 13, 180–186, 2012.

Nakayama, H., Leitl, B., Harms, F., and Nagai, H.: Development of local-scale high-resolution atmospheric dispersion model using large-eddy simulation. Part 4: turbulent flows and plume dispersion in an actual urban area, Journal of Nuclear Science and Technology, 51, 626–638, 2014.

Nakayama, H., Takemi, T., and Nagai, H.: Development of LO cal-scale H igh-resolution atmospheric DI spersion M odel using L arge-E ddy S imulation. Part 5: detailed simulation of turbulent flows and plume dispersion in an actual urban area under real meteorological conditions, Journal of Nuclear Science and Technology, 53, 887–908, 2016.

Naughton, J., Balas, M., Gopalan, H., Gundling, C., Heinz, S., Kelly, R., Lindberg, W., Rai, R., Saini, M., and Sitaraman, J.: Turbulence and the isolated wind turbine, in: 6th AIAA theoretical fluid mechanics conference, p. 3612, 2011.

Neggers, R. A., Siebesma, A., and Heus, T.: Continuous single-column model evaluation at a permanent meteorological supersite, Bulletin of the American Meteorological Society, 93, 1389–1400, 2012.

https://doi.org/10.5194/wes-2024-12
Preprint. Discussion started: 13 February 2024

Niu, G.-Y., Yang, Z.-L., Mitchell, K. E., Chen, F., Ek, M. B., Barlage, M., Kumar, A., Manning, K., Niyogi, D., Rosero, E., et al.: The community Noah land surface model with multiparameterization options (Noah-MP): 1. Model description and evaluation with local-scale measurements, Journal of Geophysical Research: Atmospheres, 116, 2011.

Porté-Agel, F., Bastankhah, M., and Shamsoddin, S.: Wind-turbine and wind-farm flows: A review, Boundary-layer meteorology, 174, 1–59, 2020.

Prusa, J. M., Smolarkiewicz, P. K., and Wyszogrodzki, A. A.: EULAG, a computational model for multiscale flows, Computers and Fluids, 37, 1193–1207, https://doi.org/https://doi.org/10.1016/j.compfluid.2007.12.001, 2008.

Rohli, R. V. and Li, C.: Atmospheric Stability and Potential Temperature, pp. 77–90, Springer International Publishing, Cham, https://doi.org/10.1007/978-3-030-73093-2_8, 2021.

Skamarock, W. C., Klemp, J. B., Dudhia, J., Gill, D. O., Liu, Z., Berner, J., Wang, W., Powers, J., Duda, M., Barker, D., et al.: A description of the advanced research WRF version 4, NCAR tech. note ncar/tn-556+ str, 145, 2019.

Smolarkiewicz, P. K. and Dörnbrack, A.: Conservative integrals of adiabatic Durran's equations, International journal for numerical methods in fluids, 56, 1513–1519, 2008.

Smolarkiewicz, P. K. and Margolin, L. G.: MPDATA: A Finite-Difference Solver for Geophysical Flows, Journal of Computational Physics, 140, 459–480, https://doi.org/https://doi.org/10.1006/jcph.1998.5901, 1998.

Smolarkiewicz, P. K. and Margolin, L. O.: On forward-in-time differencing for fluids: Extension to a curvilinear framework, Monthly Weather Review, 121, 1847–1859, 1993.

Smolarkiewicz, P. K. and Pudykiewicz, J. A.: A class of semi-Lagrangian approximations for fluids, Journal of Atmospheric Sciences, 49, 2082–2096, 1992.

Smolarkiewicz, P. K., Sharman, R., Weil, J., Perry, S. G., Heist, D., and Bowker, G.: Building resolving large-eddy simulations and comparison with wind tunnel experiments, Journal of Computational Physics, 227, 633–653, https://doi.org/https://doi.org/10.1016/j.jcp.2007.08.005, 2007.

Stauffer, D. R. and Seaman, N. L.: Use of four-dimensional data assimilation in a limited-area mesoscale model. Part I: Experiments with synoptic-scale data, Monthly Weather Review, 118, 1250–1277, 1990.

Troldborg, N., Sørensen, J. N., and Mikkelsen, R.: Actuator line simulation of wake of wind turbine operating in turbulent inflow, in: Journal of physics: conference series, vol. 75, p. 012063, IOP Publishing, 2007.

Veers, P., Bottasso, C. L., Manuel, L., Naughton, J., Pao, L., Paquette, J., Robertson, A., Robinson, M., Ananthan, S., Barlas, T., et al.: Grand challenges in the design, manufacture, and operation of future wind turbine systems, Wind Energy Science, 8, 1071–1131, 2023.

Vollmer, L., Steinfeld, G., Heinemann, D., and Kühn, M.: Estimating the wake deflection downstream of a wind turbine in different atmospheric stabilities: an LES study, Wind Energy Science, 1, 129–141, https://doi.org/10.5194/wes-1-129-2016, 2016.

Wharton, S. and Lundquist, J. K.: Atmospheric stability affects wind turbine power collection, Environmental Research Letters, 7, 014 005, https://doi.org/10.1088/1748-9326/7/1/014005, 2012.

Wildmann, N., Päschke, E., Roiger, A., and Mallaun, C.: Towards improved turbulence estimation with Doppler wind lidar velocity-azimuth display (VAD) scans, Atmospheric Measurement Techniques, 13, 4141–4158, https://doi.org/10.5194/amt-13-4141-2020, 2020.

Wildmann, N., Hagen, M., and Gerz, T.: Enhanced resource assessment and atmospheric monitoring of the research wind farm WiValdi, in: Journal of Physics: Conference Series, vol. 2265, p. 022029, IOP Publishing, 2022.

WiValdi: https://windenergy-researchfarm.com.

https://doi.org/10.5194/wes-2024-12
Preprint. Discussion started: 13 February 2024

635 Wrba, L., Bührend, L., Englberger, A., Dörnbrack, A., and Widmann, N.: A stably-stratified atmospheric inflow assimilated to measured mean profiles interacting with a wind park, Conference Paper TORQUE 2024 (under review), under review.